Dewetting and pattern formation in thin polymer films as investigated in real and reciprocal space

2003 J. Phys.: Condens. Matter 15 R1549

(http://iopscience.iop.org/0953-8984/15/36/201)

INSTITUTE OF PHYSICS PUBLISHING JOURNAL OF PHYSICS: CONDENSED MATTER

J. Phys.: Condens. Matter **15** (2003) R1549–R1582 PII: S0953-8984(03)61037-4

TOPICAL REVIEW

Dewetting and pattern formation in thin polymer films as investigated in real and reciprocal space

Peter Müller-Buschbaum

TU München, Physik-Department, LS E13, James-Franck-Straße 1, 85748 Garching, Germany

E-mail: muellerb@ph.tum.de

Received 19 March 2003
Published 29 August 2003
Online at stacks.iop.org/JPhysCM/15/R1549

Abstract

The dewetting of thin polymer films and the resulting pattern formation are reviewed and previewed. Being of crucial importance for various applications, the destabilization of an initially homogeneous layer has been investigated intensively. Recently, the growing complexity of the systems under investigation introduced new questions. In this highly active research area, different complementary methods such as experiments, computer simulations and theory have yielded new insights. Particular emphasis is placed on experiments. Future perspectives are discussed in addition.

(Some figures in this article are in colour only in the electronic version)

Contents

0953-8984/03/361549+34$30.00

1. Introduction

Polymer films on top of rigid substrates have received significant attention within the last few years. Important applications in the microelectronics industry (insulating layers or photoresists), e.g. as coatings, lubricants or protective layers, are based on the presence of a homogeneous polymeric film. As regards thickness and density, a defect-free and smooth coating is desired. The morphological features of a polymer film on a solid surface depend on the nature of long and short range interactions between the polymer and the solid [1–4]. With spin coating, thin homogeneous polymer films may also be prepared on non-wetting surfaces [5, 6]. These films are unstable or metastable. A relaxation towards thermodynamical equilibrium can occur during heat loading on the polymeric layer. The destabilization process yields a rupture of the initially homogeneous film and holes result. These holes grow in lateral size, building a characteristic pattern which decays further until a stable structure is reached. Frequently, it is an assembly of polymeric drops which replaces the initial film in the final state. Dewetting has become established as the name for this process, which represents a serious limitation for many high tech applications. Many of the investigations concerning dewetting are driven by the idea that a deep understanding of the destabilization process will enable a controlled stabilization. Another research direction focuses on the creation of surface structures, making use of the dewetting as a process responsible for pattern formation.

While macroscopic films are stable, the dewetting behaviour of mesoscopic thin films depends on whether the film is unstable or metastable. On a theoretical basis, it is the sign of the curvature of the effective interface potential $f''(h)$ determining its stability. Containing short as well as long range interactions, it is defined as the excess free energy density which is necessary to move two interfaces from infinity to a certain distance h. This distance between the solid–polymer and polymer–vapour interfaces is a measure for the film thickness and is generally the order parameter of the system. A film is unstable if $f''(h)$ is negative. Otherwise it is metastable or stable. In the metastable case the system has to overcome a potential barrier in order to reach its state of lowest energy. The film ruptures due to a nucleation process. Far away from the sign reversal of $f''(h)$ it requires the presence of nucleation sites (heterogeneous nucleation) or otherwise a thermal activation can be sufficient to overcome the energy barrier (homogeneous nucleation). In contrast, an unstable film ruptures spontaneously via a spinodal mechanism. A small fluctuation in the system order parameter gives rise to an instability. In a mean field approach with simplification to linear calculations, thermally activated capillary waves at the polymeric surface grow exponentially [7]. In analogy to the spinodal decomposition of a binary blend, the fastest growth mode destroys the film, giving rise to one dominant characteristic wavevector. Anyway, the accuracy of the prediction of the boundary between unstable and metastable states depends on whether the correct form of the effective interface potential $f(h)$ is known. In addition, within a linearly unstable range, instability-dominated and nucleation-dominated subranges have to be distinguished [8, 9].

Polymer films have attracted much attention from experimentalists focusing on dewetting. In contrast to metal films, polymer films enable a tailored viscosity to be obtained by variation of the chain length and temperature. For apolar polymers on substrates, the most widely used long range part of the interaction is the non-retarded van der Waals interface potential

$$f_{\mathrm{vdW}}(h) = \frac{A_{\mathrm{eff}}(h)}{12\pi h^2}. \tag{1}$$

The effective Hamaker constant $A_{\mathrm{eff}}(h)$ replaces the common Hamaker constant A which describes a simple two body interaction. For a liquid L on top of a semi-infinite wall W, from the approximation $A_{ij} = \sqrt{A_{ii}A_{jj}}$ the effective Hamaker constant $A_{\mathrm{eff}}(h) = A_{\mathrm{LW}} - A_{\mathrm{LL}}$ is calculated to be independent of the film thickness, whereas this dependence shows up from

the addition of a top layer O with thickness d covering the substrate:

$$A_{\mathrm{eff}}(h) = A_{\mathrm{OL}} - A_{\mathrm{LL}} - \frac{A_{\mathrm{OL}} - A_{\mathrm{SL}}}{(1 + d/h)^2}. \tag{2}$$

It accounts for a more complex substrate structure as introduced by coating layers [10]. A positive Hamaker constant repels the interface and favours a thick wetting layer of the polymer film. The interested reader will find further information concerning wetting in the reviews by Findenegg and Herminghaus [11], Müller and MacDowell [13] and Geoghegan and Krausch [14]. Recent work focused on the short ranged contributions in addition [15, 16]. The distortion of the density profile in the vicinity of the substrate gives rise to this part of the effective interface potential. According to the work of Müller *et al* [15], it decays exponentially as the distance between the interface and the substrate grows. The order of the decay length is set by the characteristic length scale ξ of the interface profile and the magnitude of its strength is set by the tension γ of the interface between the polymer liquid and its vapour:

$$\frac{f_{\mathrm{SR}}(h)}{\gamma} = a \exp(-l/\gamma) - b \exp(-2l/\gamma) + \exp(-3l/\gamma), \tag{3}$$

where a and b are coefficients of order unity. Short ranged forces dominate on length scales smaller than about $h \sim \xi \ln(\gamma/f(h))$. Alternatively, other model potentials of the long and short ranged contributions were chosen [16] (see the discussion in [13]). In summary, the interplay between short and long ranged forces can yield a quite complex shape of the effective interface potential with several local minima [13, 15].

Of course the phenomenon of dewetting is not restricted to polymeric layers. It affects metallic films as well as the growth of semiconductor layers [17, 18]. Anyway, within this topical review we restrict consideration to polymer films, which stimulated great progress in this field. Many new insights were gained from the simultaneous study of complementary methods, namely experiment, computer simulation and theory. In addition, within each of these methods new developments led to important progress.

From the experimental point of view a large variety of techniques were applied to the investigation of dewetting. Possible classifications are in terms of *ex situ* versus *in situ* experiments or *real space* versus *reciprocal space* measurements. The first addresses differences between snapshots and a kinetic investigation. The second is either applied in the well known surrounding of humans, the real space, or in its reciprocal. Real space techniques are based on imaging such as microscopy of scanning force microscopy (SFM). Reciprocal space techniques are scattering experiments with different probes such as light, x-rays and neutrons.

As regards the systems under investigation the early work on dewetting focused on simple homopolymers on top of solid substrates. Frequently, model systems such as polystyrene (PS) on top of silicon substrates (Si) covered with an oxide layer were examined [15, 16, 19–34]. PS seems favoured because it is well characterized, easily synthesized, well suited for thin film preparation, widely used in applications and has a moderate glass transition temperature. In addition, atactic PS shows no crystallization, is chemically inert and has a low vapour pressure in the melt like most polymers. Si has the advantages of being industrial extremely important, very well defined as regards surface roughness and purity and well accessible. The oxide layer of the silicon, being not that well controlled, is in some experiments covered with a siloxane coating [29]. Despite the debate about the underlying dewetting mechanism (spinodal dewetting versus nucleation and growth) [17, 32, 35–38], recently more complex systems have been examined. On the one hand, the homogeneous substrate can be replaced by nanoperiodic heterogeneous surfaces [39–46], polymer brushes [47–50], polymer layers [37, 38, 51–54, 56–59, 61–65] or a soft interface [66, 67]. On the other hand, the

homopolymer can be replaced by liquid crystals [40, 68–76], block copolymers [77–83], elastomers [84] or polymer blends [85–92]. In all these examples additional contributions to the excess surface free energy density as compared to the simple model system have to be taken into account.

This topical review is organized as follows. In the next section we describe the general basics of the sample preparation which is the first basic step of each experimental investigation. In section 3 we explain briefly the most important experimental techniques utilized for the observation of dewetting in real and reciprocal space. Then, in sections 4–6 we summarize the recent progress achieved. New perspectives are followed by a short conclusion.

2. Sample preparation

For every experimental investigation, the sample preparation marks the first prominent step. For dewetting experiments the cleaning of the solid substrate, the preparation of the initially continuous polymeric film and its destabilization are of great importance.

2.1. Substrate cleaning

In the last few years substrate cleaning has turned out to be more important than had been expected. Although it is the first basic step, in different experimental groups different cleaning procedures have been established [16, 19, 53, 93]. In principle, there is no limitation on the number of possible and successful substrate cleaning procedures. The basic purpose of the cleaning is the removal of surface contamination and the establishing of a reproducible and well defined substrate surface. On silicon substrates, as received from the manufacturer, the top oxide layer is hydrophilic or hydrophobic, depending on the chemicals used during the polishing of the surface. In addition frequently contaminations from dust particles or the laboratory environment are present. Without a substrate cleaning, arbitrary results as regards the dewetting of a polymer film will result.

Figure 1 shows an example of the strong influence of substrate cleaning on the stability of a polymer film. A 30 nm thick PS film was spin coated on top of a Si substrate with a 1 nm native oxide layer. Immediately before spin coating the PS:toluene solution, the substrates were cleaned following four different procedures. (a) A basic cleaning bath was used[1]. (b) The Si was used as received and only flushed with fresh toluene. (c) The substrate was stored in highly purified water (Milli-Q water). (d) The surface was wiped several times with a Kimwipe which was presoaked in toluene. The initially homogeneous film was stored in a vacuum furnace for 24 h at a temperature ($T = 140\,^{\circ}\mathrm{C}$) well above the glass transition temperature of PS. After quenching down to room temperature the resulting structures were viewed by optical microscopy (OM). Only after the basic bath treatment is no sign of dewetting detectable, the film remaining homogeneous. In contrast, the other surface treatments force a destabilization. From the tabulated values of the Hamaker constants of Si, SiOx and PS for 1 nm oxide layer thickness no instability of the PS film is expected. Thus the dewetting of the PS film results from residues of the polishing (b), an increased surface roughness (c) or the deposition of polydimethylsiloxane (PDMS) grains (d). All act as nucleation sites for a dewetting of the PS film. The different stages of the dewetting which were reached by using a modified surface

[1] The Si substrates were placed in dichloromethane in an ultrasonic bath for 5 min and rinsed with Millipore water shortly after. To clean the surface of organic traces the Si substrates were stored for 2 h in an oxidation bath, at 75 °C, consisting of 1400 ml Millipore water, 120 ml H_2O_2 and 120 ml NH_3. Thereafter the samples were stored in Millipore water. Directly before spin coating, the Si substrates were rinsed with Millipore water at last five times to remove possible traces of the oxidation bath. The samples were dried using compressed nitrogen before coating the Si surface.

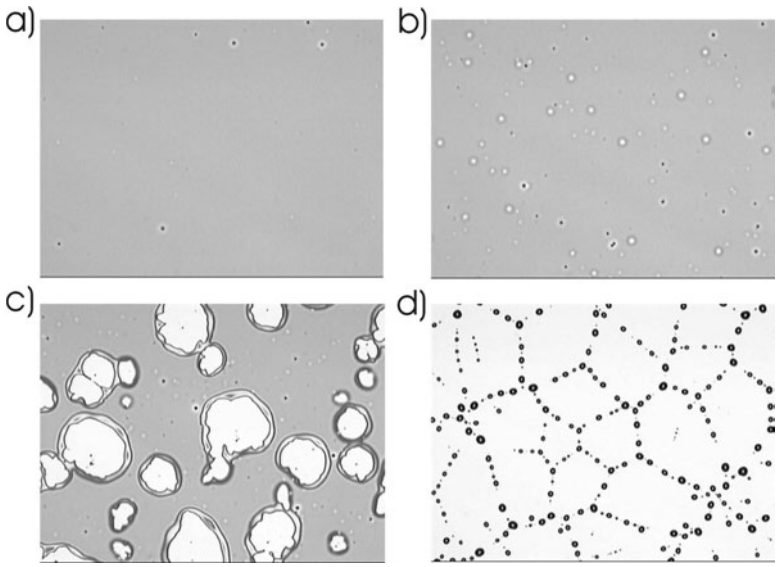

Figure 1. Optical micrographs of the surface of a PS film after annealing. The substrates were cleaned by (a) a basic etching bath, (b) flushing with fresh toluene, (c) storage for 24 h in Milli-Q water and (d) wiping with a toluene soaked Kimwipe immediately before spin coating the PS layer. While the PS film appears in grey, the Si surface reflects more light and looks white. Each micrograph shows a surface size of $625 \times 469\ \mu m^2$.

treatment can be transformed into a time span after the onset of destabilization. For indicating the density and strength of the nucleation sites, PDMS, usually used as a dewetting agent, is obviously the most effective.

Other cleaning procedures based on an acid bath[2] or using a snow-jet (a fast CO_2 jet consisting in part of CO_2 crystals)[3] [29, 30] were reported to be highly effective as well.

2.2. Film preparation

After cleaning the substrate surface, the preparation of the polymeric layer is the next step. Despite the large variety of experimental ways of placing polymer on top of a surface, the spin coating procedure turned out to be most effective. It gives rise to non-equilibrium structures and thus offers a way to prepare film on non-wettable surfaces [5, 6]. For most investigations related to dewetting, the starting condition based on a homogeneous film is most advantageous. Controlled by the preparation parameters, film thicknesses in a wide range from the submonolayer regime up to several microns may be prepared.

Due to the complex nature of the spin coating process, major simplifying assumptions had been used in the model description [5, 94, 95]. Most commonly applied is the three step model. First a polymer solution at low concentration is dropped onto the substrate, which is then started spinning. During the first step most of the solution is centrifuged off, leaving a thin layer on the substrate. In the second step the layer thins due to fluid flow until the evaporation

[2] The cleaning bath consists of 100 ml of 80% H_2SO_4, 35 ml H_2O_2 and 15 ml deionized water. After 15 min at 80 °C in the acid bath the substrates were taken out, rinsed in deionized water and dried with compressed nitrogen. Immediately before coating, the dry substrates were flushed with fresh toluene. The excess solvent was removed by one spinning cycle on the spin coater.

[3] Tectra GmBH, Frankfurt Main, Germany.

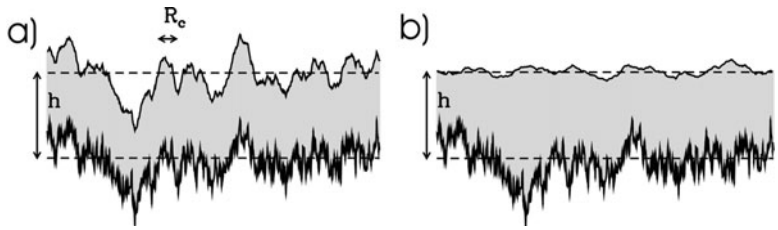

Figure 2. A schematic side-view of two interfaces at a mean distance h, corresponding to the film thickness as obtained from reflectivity experiments (the mean interface position is marked with the dashed lines). (a) The roughness spectrum of the lower interface is only transferred for in-plane length scales bigger than R_c. (b) Both interfaces are uncorrelated. The amplitude of the roughness is exaggerated for clarity.

of the solvent becomes important. The evaporation increases the viscosity of the polymer solution and slows the shear thinning of the film. During the third step, solvent is lost only by evaporation, freezing-in a thin polymer film. The resulting thickness is controlled by the initial concentration used for the spin coating [6, 96, 97] and the surface topography obtained by the solvent used [99, 100].

Even in the case of homopolymers such as PS, spin coating can give rise to marked surface structures. In an intermediate vapour pressure regime of the solvent used, such as cyclohexane, no smooth polymer surface is obtainable [99, 100]. In the regime of a small solvent vapour pressure a special polymer surface type as the ultimate lower limit of accessible surface smoothness is accessible [98, 99]. This type of morphology is called correlated roughness. A part of the roughness spectrum of the substrate is transferred through the polymer layer and determines the roughness spectrum of the polymeric surface. Just as a thin layer of snow follows the main curvatures of mountains, the polymer film can be understood as a band pass filter which transmits the long wavelength part of the substrate roughness. Figure 2(a) shows a schematic drawing of two interfaces exhibiting correlated roughness. For lateral lengths bigger than R_c the polymeric layer follows the substrate. As a consequence, for these lengths on a local scale the film has a constant film thickness. Usually a film is called homogeneous or continuous if a mean distance called the film thickness is well defined and on a local scale the height of the film deviates from this mean value (see figure 2(b)).

Experimentally, roughness correlation was observed in the case of homopolymers such as PS spin coated out of a toluene solution [93, 99, 101]. Above the entanglement molecular weight, for a large range of film thickness, spin coating gives rise to this special surface type. In addition, polymeric bilayers [102], polymer brushes [105], polymer blends [103], diblock copolymers [81] and liquid crystalline polymer films [104] exhibit this long range correlation. Annealing above the glass transition temperature results in a decay of the energetically unfavourable surface structure. Thus spin coating produces non-equilibrium films.

3. Experimental techniques

After having prepared a homogeneous polymer film on top of a solid support, the starting conditions for the experimental investigation of its dewetting are fulfilled. Most experimental works are based on a combination of several different techniques.

3.1. Real space techniques

A large body of experiments are based on imaging techniques. Operating in real space, with different levels of magnification and time needed, the surface of the polymer layer is addressed. While OM basically yields pictures of the surface, with optical phase interference microscopy (OPIM) and SFM additional height information and an improved lateral resolution result.

Starting with the early experiments and going up to recent work, OM is widely applied in research focusing on dewetting [35, 49, 50, 52, 77, 85, 106]. The advantages of a high time resolution which enables *in situ* experiments and the extremely variable magnification are reasons for its broad application. OPIM is comparable in resolution because it is based on optical light as well, but in addition gives height information [27, 28, 107–109]. Although having the advantage of being contact free, in recent investigations OPIM has been rarely applied and has been replaced by SFM [32, 48, 52, 59, 60, 68, 111]. SFM overcomes the optical resolution limit and enables the detection of the surface topography on a molecular level. It is thus well suited to detecting small changes in the surface roughness as well as to displaying the evolving changes of the surface pattern with high precision [112–114]. The time resolution is limited by the acquisition time required for the measurement of one SFM picture. However, this means no limitation for most of the dewetting experiments and thus SFM is suited for *in situ* studies as well. More serious are problems related to the tip induced surface modification during a SFM measurement or the small statistical significance of the very local SFM measurement. Knoll *et al* [115] determined quantitatively the amount of tip indentation and reconstructed the shape of the real surface of the sample in an intermittent contact mode. In order to minimize tip induced sample degradation, SFM measurements can be performed in non-contact mode. Micrographs can be recorded at different sample positions using a variety of different scan ranges to reduce the risk of a local structure information.

While SFM only probes the sample surface, which of course is strongly changed by a dewetting process, the recent development of nanotomography [117] in addition enables the detection of buried structures. Usually buried structures are addressed with scattering experiments maintaining the advantage of being non-destructive.

In the case where different phases have strongly different mechanical properties, additional information on topographical features is accessible with SFM. However, this is a very indirect method because the contrast is only a reflection of a mechanical response and not an unambiguous identification of the chemical composition. Alternative imaging techniques are scanning transmission x-ray microscopy (STXM) and photoemission electron microscopy (PEEM). In combination with near-edge x-ray adsorption fine structure (NEXAFS) techniques, a true chemical sensitivity for many polymer systems is achievable. As demonstrated by Ade *et al* [51], the dewetting of thin polymer bilayers of PS/PBrS can be measured. Between PS and PBrS no mechanical or friction difference can be detected with SFM and the bromine content in PBrS is insufficient to stain one of the phases in transmission electron microscopy (TEM). Figure 3 pictures an example of a PEEM micrograph of a dewetting PS film. The rarity of its application might be a result of the moderate resolution which, despite all the progress, still has not reached the level of SFM.

Alternatively to SFM, scanning electron microscopy (SEM) is used [53]. A meaningful lateral resolution is achieved as a result of the small source size and rather low acceleration voltages. Many polymer films, which are non-conductive in the bulk, can be imaged without coverage by a conductive material such as metal or carbon. Different polymeric materials are distinguishable without staining, which represents a major advantage in comparison to TEM. In addition to problems related to the heavy metal staining of the polymer film, microtomy carried out in order to prepare cross sections for TEM investigation forces a change in the substrate material. As an example, Si is replaced by gold coated polyimide [59].

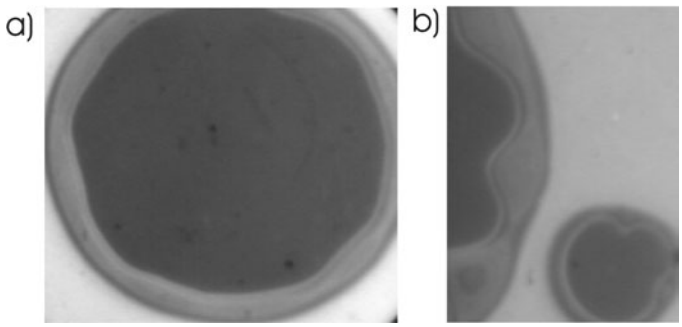

Figure 3. PEEM micrographs of the surface of a PS film on top of Si after annealing. (a) A circular hole surrounded by a rim has formed. (b) The rim exhibits modulations resulting from Rayleigh instabilities. While the PS film appears in white, the Si surface has a weaker emission and appears dark. The magnification is approximately 50 times. Reproduced with permission from [116].

3.2. Reciprocal space techniques

From scattering experiments, information in reciprocal space results. Since in a dewetting scenario, naturally a film on a solid support is under investigation, in the scattering experiments, a reflection geometry is applied. As regards the probes used, x-rays and neutrons have an advantage compared to light because their wavelengths enable a higher resolution. The incident and exit angle of the beam (x-rays or neutrons) are measured with respect to the sample surface. Depending on the values of these angles on different paths through the reciprocal space, different types of information about the sample are accessible.

In the easiest experiment, the two angles are kept equal and reflectivity is measured. Reflectivity experiments give access to the density profile perpendicular to the substrate surface [118–124]. In a non-destructive way the film thickness, which is generally the order parameter of the system, the density of the film and the surface as well as interface roughness are determined. Understanding the dewetting as a transformation of an initially homogeneous film into an assembly of polymeric drops, the density profile will be markedly changed [19, 38, 69, 107, 110, 125]. However, reflectivity experiments give no direct access to the distribution of the polymer parallel to the substrate, because the density profile is only projected information. A model is required to link a real space structure like a hole with a rim and a density profile as demonstrated by Reiter [110].

Lateral information becomes directly accessible by utilizing diffuse scattering [126–132]. For scans in which the incident and exit angle are no longer equal, the morphology is probed [38, 69, 133, 134]. In contrast to specular scattering the diffuse scattering gives rise to smaller intensities which results in the need for strong sources. In the case of grazing incidence small angle x-ray scattering (GISAXS) [12, 135], the power spectral density function of an effective surface is directly probed. With the ongoing progress in the development of advanced scattering techniques, improved access to the structures created during the dewetting results [24, 25]. In addition to the pure surface information, buried structures are detected too. Due to the quite large illuminated surface area, in a scattering experiment typical lengths are determined with a high statistical significance. Due to the loss of the phase information in most of the scattering experiments, no direct backtransformation into real space is possible. As a consequence, in contrast to the case for imaging techniques, only dominant lengths are easily determinable and no direct topography is obtained. Because in scattering experiments with x-rays and neutrons the probed length scales match well with SFM ones, a direct comparison

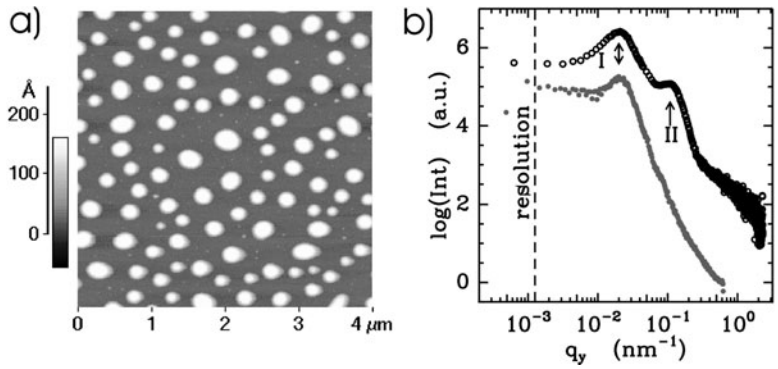

Figure 4. (a) An SFM picture of the dewetted poly(styrene-block-isoprene) film on top of Si. (b) Comparison between the master curve calculated from the SFM data (filled circles) and the GISAXS data (open circles). The mean distance between the droplets gives rise to a structure factor peak at the position labelled 'I'. Only in the GISAXS does the internal structure resulting from a microphase separation give rise to a peak labelled 'II'. The dashed lines depict the resolution limit. In this double logarithmic presentation the curves are shifted along the *y*-axis for clarity.

of the topography as determined with SFM with the results of the scattering experiment can overcome this problem [26, 89].

Figure 4 shows the example of a dewetted diblock copolymer film of poly(styrene-block-isoprene) (P(S-*b*-I)) on top of Si. With SFM the surface appears to consist of droplets. From GISAXS in addition the internal microphase separation structure inside the droplets is determined [136]. In addition GISAXS detects the mean distance between the droplets too and thus proves the statistical significance of the SFM data yielding the master curve.

In contrast to imaging techniques, advanced scattering experiments are no longer laboratory experiments, but restricted to large scale facilities such as synchrotron radiation and neutron sources. With the high flux of these sources, time resolved experiments which address the kinetics become possible. In addition problems caused by radiation damage mark limitations on increasing flux or increasing time resolution.

4. Dewetting stages

Starting with a homogeneous film, its subsequent dewetting can be divided into several different stages. In each stage different typical experimental observations were reported.

4.1. Early stages

A thin film prepared by spin coating might exhibit roughness correlation right after preparation, irrespective of the type of polymer used. During annealing this correlation decays and the liquid polymer surface is dominated by thermally excited waves. The spectrum of these so-called capillary waves gives rise to a surface roughness which is of the order of a few ångströms only, because of the restoring force of the surface tension. As demonstrated by Kerle *et al* [137] an artificially roughened PS surface smooths itself. A partial relaxation of the surface asperities at temperatures well below the bulk glass transition temperature was observed. As long as the effective interface potential stabilizes the liquid surface, the film remains homogeneous. An example system with a stable thin homopolymer layer is brominated PS. A change of the cut-off wavevector q_c defining the correlated part of the surface roughness from a $q_c \sim h^{-0.5}$ to a $q_c \sim h^{-2}$ behaviour was determined [101]. Thus during annealing the surface morphology

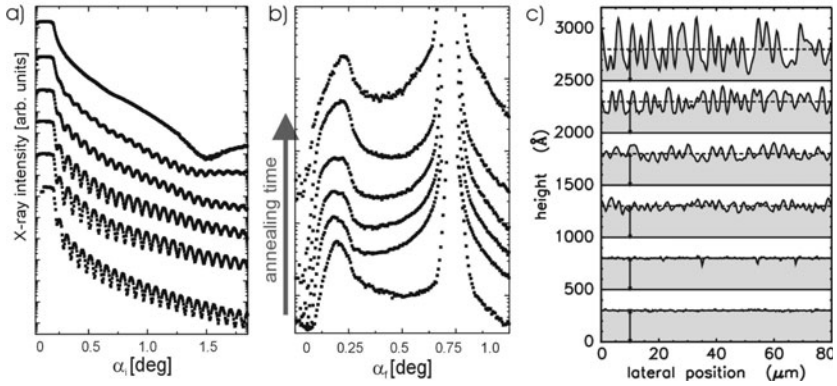

Figure 5. *In situ* investigations of the dewetting of a thin PS film with a thickness of 59 nm on top of Si with (a) x-ray reflectivity and (b) diffuse scattering exhibit marked changes even during the early stages. All curves are shifted for clarity along the y-axis (annealing time increases from the bottom to the top). (c) Dewetting of a diblock copolymer film followed by SFM. Line scans from SFM data measured after different annealing times (increasing from bottom to top). Note that the scalings of the x-axis, displaying the lateral sample position, and the z-axis, displaying the height, are different by a factor of $\widetilde{=}250$ to emphasize the surface topology. In addition the line scans are shifted by 500 Å against each other along the z-axis to enable picturing of the evolving structures with increasing annealing time from the bottom to the top. The mean surface height as determined with x-ray reflectivity is visualized with the dashed lines and the film volume is plotted in grey. Reproduced with permission from [82].

changes from a frozen-in liquid into an interaction controlled one. With increasing roughness of the underlying substrate an increasing part of the roughness spectrum is replicated by the polymeric surface in equilibrium [138]. However, in most investigations concerning dewetting the substrates are extremely smooth with typical amplitudes of the surface roughness of the order of a few ångströms as well. As a consequence, stable homogeneous polymer films exhibit very smooth surfaces.

In the case where the van der Waals interaction of the polymer molecules and the substrate atoms is small as compared to the interaction between the polymer molecules themselves, the long range part of the effective interface potential destabilizes the polymeric film. An unstable film, fulfilling $f''(h) < 0$, decays via spinodal dewetting: analogous to the situation for spinodal decomposition in fluid mixtures, composition fluctuations are replaced by height fluctuations. A thermally induced thickness modulation $z(\vec{\rho}, t) = h + \delta h \exp(\mathrm{i}\vec{q} \cdot \vec{\rho})$ on a homogeneous film with a thickness h grows over time t. The coordinate parallel to the surface is denoted as $\vec{\rho}$ and the wavevector as $\vec{q}$. The surface fluctuation $\delta h = \delta h_0 \exp(t/\tau(q))$ is determined by a wavelength $\Lambda = 2\pi/|\vec{q}|$ and a relaxation time $\tau(q)$. In the linearized model the initial fluctuations are amplified exponentially in the case where the wavevector is smaller than a critical wavevector q_c [7, 139]. This corresponds to an increase of the surface roughness following $\sigma \sim \exp(-t/T)$, which is one characteristic feature of the early stages of the dewetting process. Among all unstable modes, the fastest growing mode with a wavevector $q_m = \sqrt{(3/2)}(a/h^2) = q_c/\sqrt{2}$ destroys the film. The relaxation time of the instability $\tau_m = \pi\eta h^5/(6a^2)$ depends strongly on the initial film thickness h, where η denotes the viscosity, γ the surface tension and a a molecular length which depends on the van der Waals interaction [7, 139, 140]. Experimentally the rupture time is extremely difficult to measure, because the hole created must have a certain diameter to become observable to the experimentalist.

As a consequence work on the early stages focuses on the increase of the surface roughness. Scattering and SFM enable the detection of this increase as shown in figure 5. The scattering data indicate the roughening of a 59 nm thick low molecular weight PS film ($M_w = 1.75$k) on top of Si with its native oxide layer. *In situ*, during annealing, the changes in the reflectivity and in the diffuse scattering were monitored. In the reflectivity data first the thermal expansion of the PS film becomes visible via the decrease of the wavelength of the fringes. Next the amplitude of the fringes is damped which results from an increase of the surface roughness. From the fit to the data an exponential increase of the rms surface roughness σ was observed [141]. Correspondingly, in the diffuse scattering the shape of the Yoneda peak [142], located at $\alpha_f \sim 0.2°$, contains information about the lateral roughness in terms of characteristic wavelengths on top of the surface. Within the required modelling of the scattering data the prediction $\sigma \sim \exp(-t/T)$ of the spinodal model is fulfilled. However, without a real space analysis important information is missing.

Of special interest is the installation of a preferred wavelength $\Lambda = 2\pi/q_m$. Within the spinodal model the value of this dominant wavelength depends on the film thickness $\Lambda \sim h^2$. Xie *et al* [32] detected a bicontinuous surface pattern for thin low molecular weight PS films ($M_w = 4.0$k, $h < 10$ nm) on Si with a native oxide layer with SFM. The exponential increase of the surface amplitude as well as the characteristic lateral length scales of the surface modulations matching $q_c/q_m \cong \sqrt{2}$ fit to a spinodal dewetting scenario. With increasing film thickness a qualitative change in the behaviour was observed, which prevented the verification of the scaling with respect to the order parameter. At larger film thicknesses holes resulting from nucleation were observed. Because the pure long range part of the interaction does not predict an instability of PS on Si with a thin oxide layer, use of the system PS/SiOx/Si might be questionable for the proof of spinodal dewetting.

Seemann *et al* [16, 30] investigated the influence of the oxide layer thickness. For low molecular weight PS ($M_w = 2.05$k) on Si with a thick thermally oxidized SiOx layer (thickness 191 nm) the condition $f''(h) < 0$ is fulfilled. With SFM the typical decay of the bicontinuous surface pattern was observed and the resulting increase of the surface amplitude fits to an exponential growth for the early stage. In addition the characteristic wavelength behaves in accordance with the spinodal model. On Si substrates with a native oxide layer of common and small thickness of the order 1.7 nm no sign of a spinodal dewetting was detected [16]. In an intermediate regime of oxide layer thickness again a preferred wavelength was found for PS film thickness smaller than 4.1 nm. From the reconstructed effective interface potential this was attributed to a homogeneous (thermal) nucleation process.

Replacing PS by more complex polymers such as liquid crystals [68–70, 72–76] or block copolymers [77–83] gave rise to a destabilization which was reported to result from a spinodal dewetting process as well. Herminghaus *et al* [40, 70] followed the dewetting of a liquid crystalline tris(trimethylsiloxy)silane-ethoxy-cyanobiphenyl film. Initially a Langmuir film was prepared by spreading the material on deionized water. After transfer to Si dewetting occurs within just a few minutes. Figure 6 displays the resulting surface structures as a snapshot at one fixed time. In addition to the bicontinuous pattern which was taken as a fingerprint of a spinodal process, circular holes appear. These holes were attributed to a nucleated dewetting and thus figure 6 pictures nicely the two competing dewetting mechanisms, namely spinodal dewetting and nucleation.

In contrast to the global destabilization due to spinodal dewetting, in a nucleated dewetting a defect on a local scale destabilizes the polymer film. Depending on the strength of the defect, a critical radius r_c of the hole created, which destabilizes the film, results [143, 144]. Holes with a smaller radius $r < r_c$ will be annealed and no dewetting is observable, although locally the surface is not wettable. In a simple approximation, the critical hole radius $r_c =$

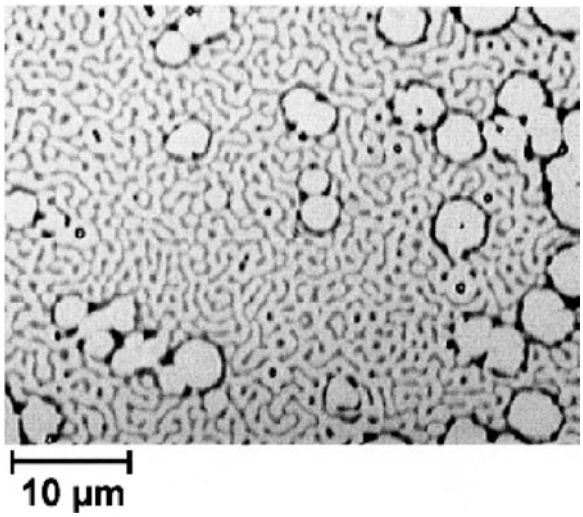

Figure 6. An optical micrograph of a liquid crystalline tris(trimethylsiloxy)silane-ethoxy-cyanobiphenyl film after transfer from the Langmuir trough onto Si. At room temperature both circular holes nucleated from defect and an undulative mode are visible. Reproduced with permission from [40].

$h(1+\sqrt{2})/(1-\cos\theta)$ depends on the film thickness and the contact angle [144]. Simulations by Liu *et al* [145] exhibit the existence of a critical hole radius as well. Experimentally, artificial holes created with a SFM tip were investigated. Karapanagiotis *et al* [146, 147] determined the influence of artificial defects for PS ($M_w = 10.9$k, $h < 100$ nm). For the different substrates, with increasing contact angle the value of the critical radius reduces [141]. For example on native oxide covered Si surfaces compared with OTS silanized Si surfaces, the critical radius is approximately five times larger. Thus on native oxide, Si nucleation is less likely or in other words defects have to be five times larger to give rise to a destabilization.

However, the nature of the defect yielding the destabilization can be of different origin. Dust particles and Si fragments, resulting from the cracking of the Si substrates (preferentially at the edges of the Si pieces), are easily observable by imaging techniques. Located inside the centre of a dewetted patch [148], these defects can be reduced in number by improvement of the preparation conditions. Grains below the optical resolution limit such as impurities from the solvents used, PDMS from fuzz-free wipes and other polymers giving rise to a negative Hamaker constant are much more difficult to detect. Again, an improvement of the preparation conditions will reduce the number density of these defects as well. But, besides all nucleation effects related to impurities, defects can result from the thin film preparation itself. Strain induced by the preparation via spin coating is discussed as an additional origin [149, 150]. Spin coating PS out of a toluene solution introduces an internal stress of the order of 14 MPa [151]. For other solvent/polymer combinations values of a comparable order will result. In addition at least for high molecular weights non-equilibrium chain conformations have to be considered [150].

The absence of the film thickness dependence of the characteristic wavelength as predicted in the spinodal model and the presence of a dependence on the heating rate instead was taken as proof of a nucleation process [71]. One other possibility for distinguishing between the global spinodal dewetting and a more local nucleated dewetting is based on integral geometrical methods, namely using Minkowski functionals [35, 70, 152, 153]. This versatile method for

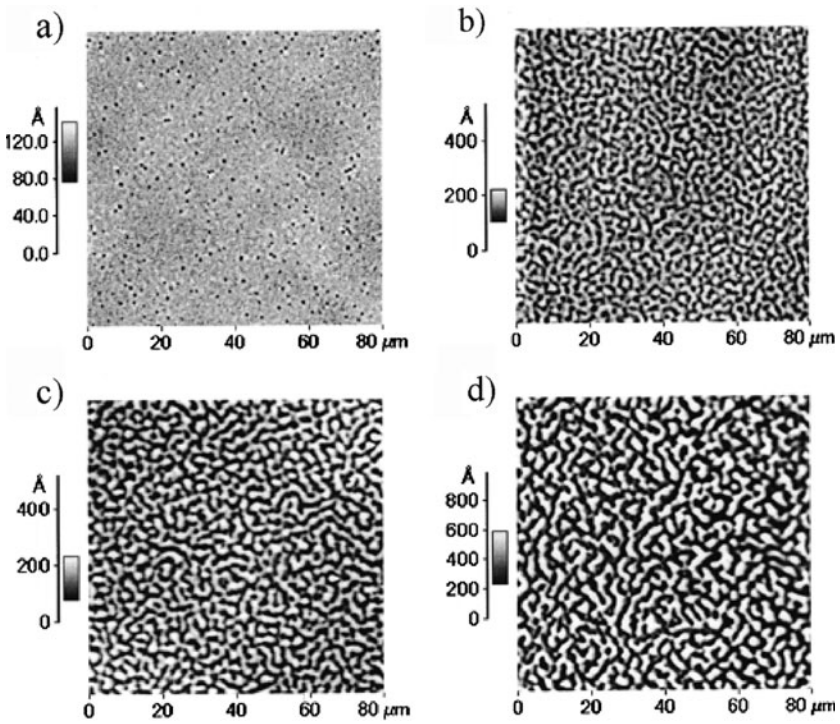

Figure 7. Dewetting of a thin P(S-*b*-pMS) diblock copolymer film: SFM pictures (scan range 80×80 μm^2) of the topology signal as observed after annealing for (a) 284.5 h, (b) 400 h, (c) 725.5 h and (d) 1874 h. The height scalings are different for each pattern, to show the in-plane structure more clearly. Reproduced with permission from [82]. Copyright 2002 American Chemical Society.

tracking down higher order correlations is successfully applied at the end of the early stages, at which holes have formed. It is thus best suited for experimental investigations in which the preferred wavelength cannot be detected by Fourier transformation before the film ruptures. In two dimensions a possible set of Minkowski functionals is given by the area F, the boundary length U and the Euler characteristic χ of the coverage [153]. The latter is defined as the integral over the boundary curvature yielding the connectivity of a structure. Resulting from the random arrangement of grains on a sample surface, holes due to nucleation are randomly distributed. Following a Poisson statistics, the corresponding Minkowski functionals are markedly different from the ones resulting from a spinodal process as shown by Jacobs *et al* [35, 152]. As an example of the dewetting of PS on Si with a native oxide layer, heterogeneous nucleation was identified as the mechanism responsible for the symmetry breaking.

The dewetting of the diblock copolymer poly(styrene-block-paramethylstyrene) diblock (P(S-*b*-pMS)) from native oxide covered Si enables the detection of the change in the surface topography before the film ruptures [81, 82]. With SFM the coarsening of the bicontinuous surface undulation was measured at a film thickness below the bulk lamellar period. Figure 7 shows four snapshots at different annealing times picturing typical early stages. Figure 5(c) shows corresponding line scans from the SFM data. Starting with a homogeneous film of small surface roughness, the early stages were detected. Due to the large molecular weight ($M_w = 230$k) it was possible to measure small holes which do not rupture down to the substrate. The increase of the amplitude and wavelength with time during annealing is consistent with a spinodal dewetting process.

In more complex systems evidence for the presence of a spinodal process was observed as well. Bilayer systems enable the installation of suitable effective interface potentials. For the choice of a favourable sequence of polymer layers, a negative Hamaker constant results, yielding $f''(h) < 0$. Examples are polymethylmethacrylate (PMMA) on PS [38, 54, 55], brominated PS on PS [51], PS on PDMS [52], polycarbonate (PC) on styrene-co-acrylonitrile (SAN) [53, 59], PS on polyamide-6,I (PA) [37] or PS on the diblock copolymer polyvinylpyridine-block-polystyrene (P(VP-*b*-S)) [58]. In addition dewetting was observed in some reverted arrangements such as PS on PMMA as well [48, 57, 61, 63, 65] although the long range part of the interaction favours wetting. Depending on the chosen temperature of annealing and the molecular weights the viscosity can be controlled in addition [62].

Liquid/liquid spinodal dewetting was studied for example by Sferrazza *et al* [38]. PMMA on top of PS ($M_w = 1900$k, $h = 120$–140 nm) was investigated by means of neutron reflectivity and neutron diffuse scattering. An intermediate molecular weight ($M_w = 108$k) was used and the data were consistent with the spinodal model as regards both the length scale and the characteristic time of growth of the unstable waves. For low molecular weight PS ($M_w = 8.7$k) on PA Renger *et al* [37] observed a bicontinuous surface pattern in the case of a small PS film thickness ($h < 35$ nm). With increasing thickness of the PS film a crossover from the spinodal to a nucleated dewetting was detected. The thicker the films, the weaker the driving force and the larger the growth time of the spinodal mode. In contrast to the spinodal dewetting following $\tau_{\text{spinodal}} \sim 1/h^5$ for nucleation, a less drastic film thickness dependence $\tau_{\text{nucle}} \sim \eta/h^3$ was reported [154], where η denotes the viscosity. For thicker films, dewetting by heterogeneous nucleation may therefore be quicker and suppress the appearance of the spinodal process [155].

A special case of a bilayer scenario results from a chemical anchoring of the polymers of the sublayer onto the substrate. Yielding a brush, the interface energies are changed and polymers can even dewet on top of a layer of identical but grafted molecules [58, 107]. This behaviour is similar to the cross-link induced autophobicity in polymer melts, in which a polymer dewets a brush-like surface of the network of the same polymer as investigated by Kerle *et al* [156, 157]. Increasing the cross-linking densities or choosing a bimodal brush instead of a monomodal brush by adding chains with a higher molecular weight and thus larger chain length can re-establish wettability [156, 158]. The long chains act as connectors across the non-wettable interface. The part of the dense brush of short chains underneath the connectors prevents contact of the free polymer molecules of the top layer and the chemically different substrate atoms such as Si.

Figure 8 shows the example of a 41 nm thick PDMS film on top of a bimodal brush of PDMS anchored on a Si substrate by Reiter *et al* [50]. The addition of a 1 mm thick layer of water on top of the PDMS marked the starting condition $t = 0$ and inverted the sign of the Hamaker constant yielding an instability of the PDMS melt. A bicontinuous undulation pattern is observed by OM. The reduced contrast results from the reduction of the refractive index contrast due to the water layer. The lateral features do not change in the beginning (compare figures 8(A) and (B)), except that there is an improvement of the contrast, which indicates that it is mainly the amplitude of the surface modulation and not its wavelength that increases. The removal of the water layer again inverted the sign of the Hamaker constant and a re-spreading was observed (compare figures 8(E) and (F)). Finally a smooth film of PDMS was re-established again [50]. This shows that films which are stable in air are not necessarily stable if the bounding medium is changed.

In addition Reiter *et al* [159] recently showed that this special system is well suited for tuning the kinetics of the film stabilization to a limit which enabled the investigation of the time of rupture. Relying on theoretical considerations [7, 139, 160, 161] experimental data

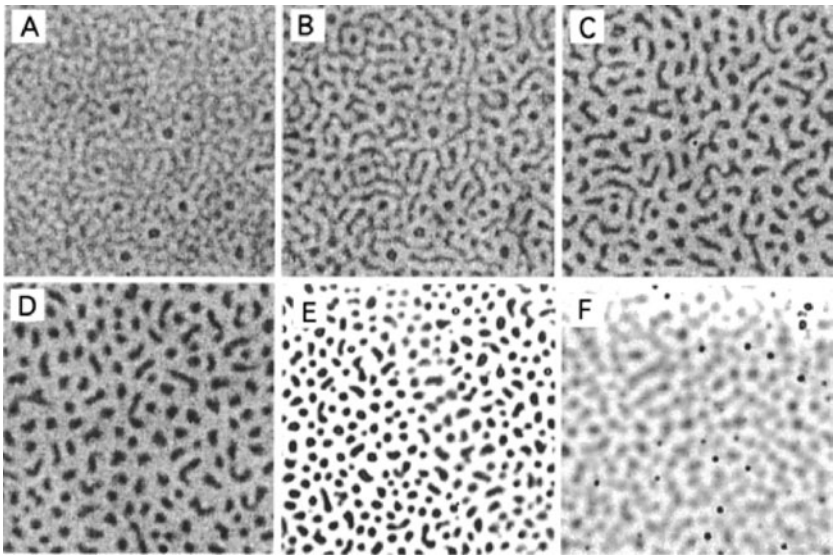

Figure 8. Optical micrographs picturing the dewetting of PDMS after (A) 39 s, (B) 88 s, (C) 211 s, (D) 395 s, (E) 656 s and (F) 680 s. At time $t = 0$ s a millimetre thick water layer was put on top. The size of each micrograph is $200 \times 200\ \mu m^2$. The greyscale covers a thickness regime from zero (white) to about 100 nm (black). After 650 s the water layer was removed yielding a re-spreading of the PDMS. Reproduced with permission from [50]. Copyright 1999 American Chemical Society.

from different viscosities η and interfacial tensions γ were superposed on one master curve which obeyed $\tau \sim \eta\gamma h^5$.

4.2. Hole growth and rim

At the end of the early stages isolated holes have formed in an otherwise uniform film. The material displaced from the dewetted area has to be moved elsewhere due to mass conservation and the non-volatile character of polymers. Either it is accumulated into thicker regions around the hole, yielding a so-called rim [53, 92, 162], or it is distributed almost evenly within the whole film in between the holes [163].

Figure 9 depicts two corresponding examples as visualized with SFM. In both cases nucleation was artificially caused by the addition of impurities deposited on top of the substrate, since nucleated holes show nicely characteristic features. As figure 9 suggests, the holes in a homopolymer film (PS with $M_w = 27.5$k, $h = 41$ nm) differ in shape from holes in a diblock copolymer film (P(S-*b*-I) with $M_w = 13.0$k, $h = 60$ nm).

The initially opened up holes grow in size during further annealing. Because the surface 'prefers' to be dry, a negative spreading coefficient $S = \gamma(\cos\theta - 1)$ originates this growth. At the contact line, typical values are in the case of air/PS/Si $S = -0.3$ mN m^{-1} and for air/PS/OTS-Si $S = -15$ mN m^{-1} [149]. As regards the subsequent hole growth many different systems were addressed by experiments. Triggered by the theoretical models [164–167] the dewettings on top of a solid support [30, 35, 36, 52, 70, 77–79, 163, 168–172] and on a liquid support [37, 48, 57, 59, 61, 63] can be distinguished.

On a solid surface an ideal Newtonian liquid exhibits a different movement as compared to an entangled polymer melt. A flowing liquid dissipates energy by viscous friction (the so-called no-slip regime). The highest shear rate is at the three phase contact line and the contact angle stays constant. As a consequence the spreading coefficient is constant and the radius r of

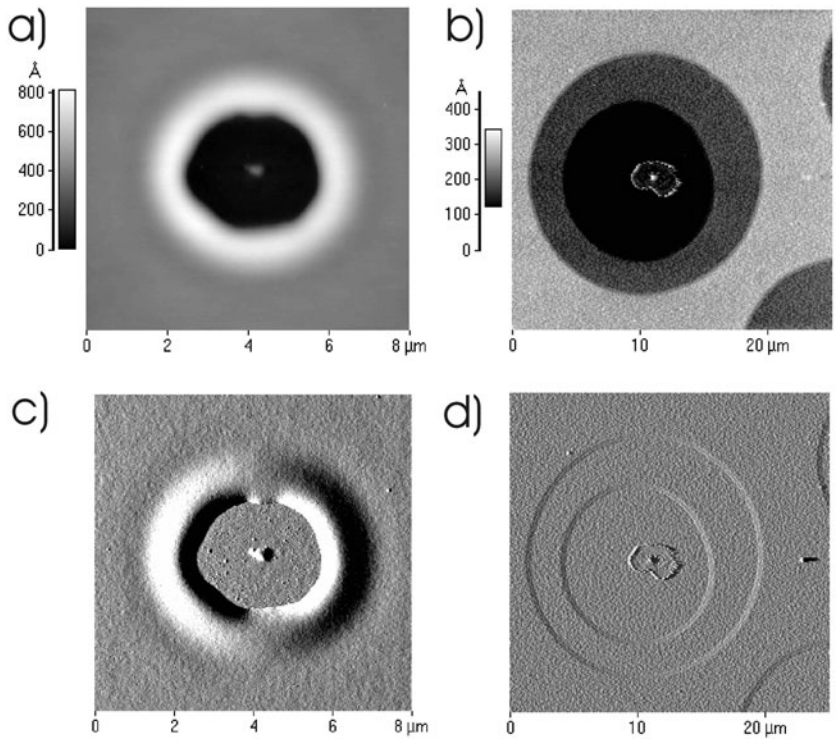

Figure 9. SFM pictures of nucleated holes in an ((a), (c)) 41 nm thick PS film and a ((b), (d)) 60 nm thick P(S-*b*-I) film. The film dewetted from artificially deposited grains. The grains remain visible inside the hole and cause an increase of the height in the hole centre. The ((a), (b)) topography and the ((c), (d)) error signal are shown for comparison.

the hole grows with a constant velocity $\mathrm{d}r/\mathrm{d}t = v$ giving rise to an $r \sim t$ [165, 172] behaviour. In contrast an entangled polymer melt belongs to the full-slippage regime and the velocity at the solid surface is larger than zero. The slippage is characterized by an extrapolation length b, defining a distance below the solid surface at which the velocity would extrapolate to zero. In thin films with $h < b$ the polymer slides comparably to a solid and viscous dissipation is confined to the solid/liquid interface. As a result the hole growth follows $r \sim t^{2/3}$.

When considering a liquid substrate (liquid/liquid dewetting), the substrate viscosity must be taken into account. The dewetting velocity depends on the relation between the viscosity of the polymer layer η_f and the substrate η_s. For $\eta_\mathrm{f}/\theta < \eta_\mathrm{s}$ (θ denoting the contact angle between film and substrate) the hole grows according to $r \sim t$. For $\eta_\mathrm{f}/\theta > \eta_\mathrm{s}$ however, the area grows as $r \sim t^{2/3}$. Thus, for liquid/solid as well as for liquid/liquid dewetting, the values 1 and $2/3$ mark the limits of the exponent of hole growth. In experiments on real polymer films deviations from both limiting cases were reported.

Jacobs *et al* [36] presented an interpolation between the two limiting cases of perfect sticking and full slippage which was able to explain the data measured for PS films ($M_\mathrm{w} =$ 16–600k) on silanized Si. The friction contribution was ruled to be independent of PS film thickness and temperature, whereas the viscous dissipation scales like the viscosity of the liquid as regards the temperature dependence.

Reiter *et al* [107] followed the hole growth in thin PS films on top of a dense PS brush revealing a slowing down of the growth with increasing time. During the initial growth stages, the rim surrounding the hole is still small and slippage is dominant, whereas during later

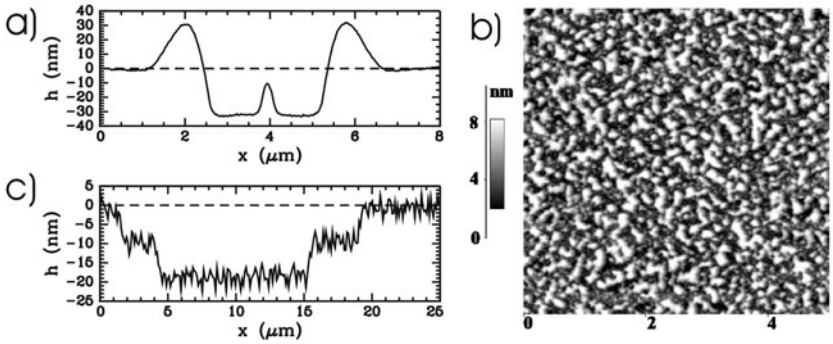

Figure 10. Line scans cut through nucleated holes in a (a) 41 nm PS film and (c) 60 nm P(S-*b*-I) film on top of native oxide covered Si. Note that the scaling of the height and the lateral axis are different to emphasize the shape of the hole. In addition (b) shows a close-up of the topography as measured with SFM on top of one terrace of the P(S-*b*-I) film explaining the absence of a smooth line shape in the corresponding line scan.

stages the rim has increased in size and viscous dissipation becomes dominant. Consequently the exponent of the growth law changes from 2/3 to 1. In experiments related to PDMS ($M_w = 308$k, $h = 20$–850 nm) on a PDMS brush a more general fit function $r(t) \sim (t - t_0)^{\alpha}$ introducing a growth exponent α was used to explain the data [173]. Values close to $\alpha = 2/3$ indicating slipping of the polymer films were fitted.

Even for more complex polymers such as diblock copolymers Limary and Green [79] observed a growth law with a slope of 2/3. In addition in the early stages a transition from an exponential growth with $r \sim \exp(t/\tau)$, as long as a rim is absent, into a linear one was reported. Alternatively, a simple Kolmogorov growth law [174, 175] was used to explain the increase of the hole area of individual holes created by a controlled nucleated dewetting of a PS ($M_w = 8.7$k, $h = 19$–28 nm) film from Si with its native oxide layer [23].

In polymeric bilayers such as PS on PMMA [48, 57] the viscosity of the substrate (the sublayer) becomes tunable. On liquid substrates a competition of mass transport in the substrate and the retarded deformation of the liquid–liquid interface changes the dewetting velocity and yields a minimum as a function of the molecular weight [57]. With cross sections through SFM images the deformation of the sublayer was detected [48]. On highly viscous substrates of PA the growth exponent α was probed as a function of the PS ($M_w = 2.2$k and 8.7k) top layer thickness by Renger *et al* [37]. For thin but still unconfined films of the order of $5R_g$ in size a significant increase of α was observed. In the reverted case a highly viscous layer dewets from a liquid one [163]. If both layers are sufficiently above their glass transition temperatures a liquid/liquid dewetting becomes observable. For PC dewetting from SAN a linear growth with $\alpha = 1$ was observed.

In addition to the total growth of the dry area increasing attention is attracted by the individual shape of the rim surrounding the hole. Figure 10 shows line scans which depict the shape of the hole for both types of hole introduced in figure 9. Obviously two different kinds of hole are present: the hole in the PS film is surrounded by a well developed rim and exhibits a smooth surface. In contrast the hole in the P(S-*b*-I) film is not accompanied by a rim and has a terrace shape and a rough surface. This roughness resulted from an additional microphase separation structure yielding a grainy surface as displayed in figure 10(c).

Taking into account the elastic properties of the polymer film, different morphologies of the rim were calculated. Herminghaus [176] identified three clearly distinguishable types of rim. For PS with a large molecular weight ($M_w = 600$k, $h = 40$ nm) the rim is asymmetric with a

steep incline starting from the dry area, a crest and a smooth decay towards the remaining part of the film. With decreasing molecular weight (e.g. $M_w = 101$k) it is mainly the steepness that increases. However, within this range of molecular weights a double exponential fit explains the profile. At a drastically smaller molecular weight ($M_w = 2$k, $h = 4.9$ nm) the profile becomes oscillatory. The decay towards the remaining film is superimposed on by an oscillation, meaning that the height of the film is reduced close to the rim. A further reduced film thickness ($h = 3.9$ nm) finally results in a cascade of polymeric material. Because the film is thin enough, the ditch can reach the substrate and pinch off the crest from the film, building a new contact line [176]. From several repetitions of this process a series of isolated crests result which appear as a cascade of polymeric material.

As expected theoretically [165] and observed experimentally [59, 79, 173, 178, 179] the dewetting of a viscous liquid gives rise to a quite symmetric rim with a double exponential shape. The profile shown in figure 10(a) exhibits a quite symmetric rim as well and in addition a small ditch near the rim towards the wet, homogeneous film. The more complex patterns resulting from the oscillatory or cascade decay were measured and simulated in the case of thin PS films on thermally oxidized Si [182]. Alternatively it was observed in an initially flat film which was scratched artificially with a SFM tip, producing a dry channel [183]. During the subsequent annealing of the unstable film, satellite holes result from the cascade pattern. The positions at which the satellite holes appear correspond to positions on the wet side of the rim where the film thickness was smaller. This reduction of the film thickness on the wet side resulted from the trough which had initially formed. The presence of the trough was attributed to a local negative curvature of the film surface. Consequently flow occurs from the region of higher generalized Laplace pressure to the surrounding film, causing a ditch first, and a secondary hole finally [183]. The repetition of this process results in a typical cascade of polymeric material. For a slightly larger film thickness of the PS layer, the ditch is not deep enough to reach the substrate and a pure oscillatory rim shape is present, as observed by Seemann *et al* [162]. Qualitatively the development of the height of the rim with respect to the depth of the trough was achieved. From the molecular weight dependence the alteration of the shape of the rim was attributed to the increase of viscoelastic properties, such as the ratio of viscosity and elastic modulus at the typical shear rates to which the material is subjected upon dewetting [162].

At the early stages holes in a PS film on a PDMS brush grew independently of the molecular weight of the polymer and without the formation of a rim [163]. Instead of accumulating material near the hole by the building up of a rim, the complete film in between the holes increased in its thickness. Comparably with x-ray reflectivity results, a thickening of the film without a significant roughening was detected by Orts *et al* [177] for PS on Si. At later stages a rim built up. It has a highly asymmetric shape with an extremely steep depression towards the dry area and a much slower decay towards the homogeneous film. The maximum height increases linearly with the diameter of the hole. Because annealing was performed in [163] close to the glass transition temperature of the bulk PS, the polymer was highly elastic, preventing viscous flow. A plastic deformation was attributed to destruction of the thin, initially homogeneous quasi-solid film. This experimental finding is supported by the observation of a fibrillar craze-like structure at the contact line [171]. Theoretically the dewetting of thin polymer films near the glass transition including shear thinning is discussed in [180, 181].

The absence of a rim surrounding the dry patch was observed in the case of more complex systems as well. For two different diblock copolymers P(S-*b*-MMA) [78–80] and P(S-*b*-pMS) [82] small holes exhibit no rim, whereas after a longer annealing time a rim was formed. In the case of P(S-*b*-I) even larger holes are not surrounded by a rim, but a terrace-like structure is installed. Depending on the special type of diblock copolymer chosen

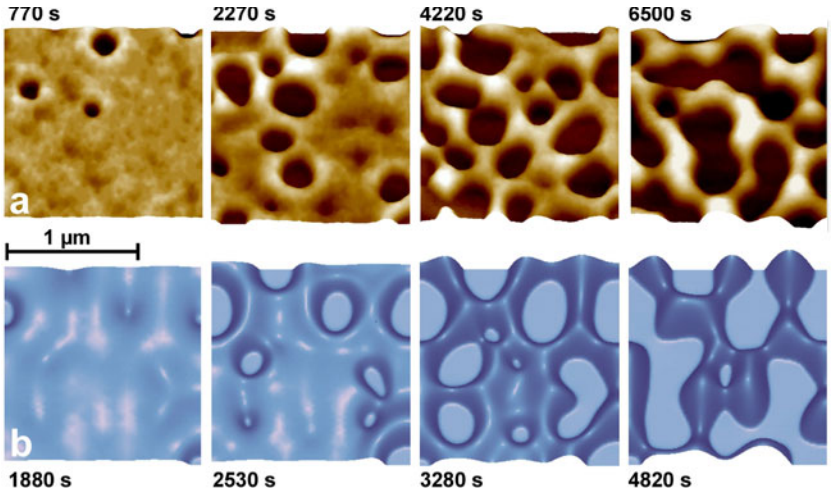

Figure 11. Comparison between (a) an experimentally observed time series of dewetting morphologies in the system PS ($h = 3.9$ nm) on top of oxidized Si and (b) a simulated one with the same system parameters as in the experiment. Annealing was performed at 53 °C. Highest points reach 12 nm above the hole ground. Reproduced with permission from [182].

for the investigation, the surface is either smooth (comparable to the shape of homopolymers as depicted in figure 10(a)) or a lateral microphase separation structure is superimposed, which roughens the surface (see figure 10(c)).

Recently, Becker *et al* [182] achieved quantitative agreement between experiment and simulation for the full complex spatial and temporal evolution of ruptured PS films on thermally oxidized Si. Figure 11 shows data measured with SFM and from simulation in comparison. The simulation was started with a slightly perturbed film. The system was chosen to have a long wavelength instability caused by spinodal dewetting resulting from the long range interaction. Viscoelastic effects were neglected in the simulation, matching the chosen low molecular weight ($M_w = 2$k). Without a fitting parameter a time interval far exceeding the initial rupture was covered by a thin film model:

$$\eta\, \partial_t h - \nabla \cdot (m(h)\, \nabla p) = 0. \tag{4}$$

The viscosity is denoted by η, time by t, the Laplace pressure by $p = -\gamma\, \Delta h + f'(h)$, depending on the surface tension γ and the effective interface potential $f(h)$ and a non-negative mobility coefficient by $m(h)$. This coefficient captures the boundary conditions of the liquid flow (e.g. non-slip $m(h) = h^3/3$) and vanishes at $h = 0$ [182]. In addition, changes in the kinetics caused by a change of the initial film thickness of only 1 nm were covered. At a larger film thickness the correlated pattern as shown in figure 11 is replaced by the growth of an individual hole developing satellite holes as described above. In the simulation the slight perturbation of the film was set to a slight corrugation with a depression in the film centre.

4.3. Intermediate stages

In the intermediate stages adjacent holes have reached each other and as a consequence a further undisturbed hole growth is impossible. This gives rise to significant changes of the observed growth laws. The dry area increases more quickly after the merging of adjacent holes [37]. Most of the initially homogeneous film is transformed into rims surrounding the holes and

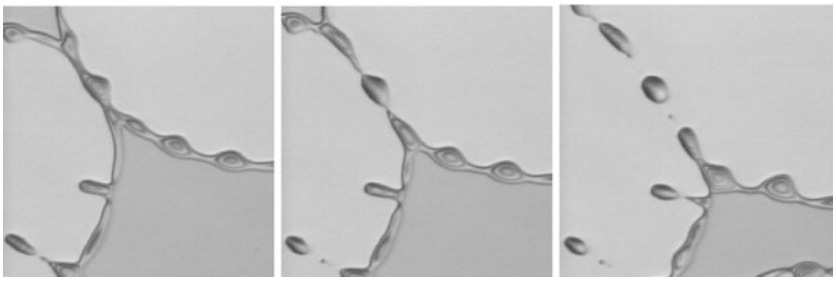

Figure 12. Time series of three optical micrographs of the surface of a PS film on top of Si during annealing showing the merging of two neighbouring holes. From the left to the right the time increases. The initially formed rim decays into drops. Reproduced with permission from [116].

instead of a coalescence of the dry patches first the rims merge. The evolving topographies of course depend on the type of rim established during the hole growth.

Figure 12 shows an example of this merging. A PS film ($M_w = 8.7$k, $h = 31$ nm) dewets from Si with a native oxide layer via a nucleation process. In addition to an instability which can be present on the rim surrounding a hole (see figure 3: the distance between adjacent swellings of the rim corresponds to the wavelength of the instability) the resulting merged rim exhibits instabilities as well. The rim can be approximated by a toroidal surface, which is similar to a cylindrical surface due to its high aspect ratio [40]. As a consequence the toroidal rim can decay into a corona of isolated drops as well. Understanding the merged rim as a liquid ribbon with a typical cross section similar to a part of a cylinder, the Rayleigh-plateau instability forces its decay into isolated droplets as well. The shape of the drops is characterized by a better ratio between volume and surface as compared to a cylinder and is thus favoured in this surface tension driven process.

The stability of liquid microchannels was investigated by Gau *et al* [184]. Unlike in the Rayleigh-plateau instability such channels tended to form single bulges as soon as the contact angle exceeded a certain characteristic value. In addition, neighbouring channels merged, if two bulges were in close proximity.

In contrast during dewetting at a certain time isolated drops, rims with Rayleigh instabilities and homogeneous films coexist, as is visible in figure 12. Due to the negative spreading coefficient during further annealing rims still move on top of the substrate and accumulate material from the remaining homogeneous parts of the film. In contrast the drops created exhibit no further movement but remain at the position where they were initially formed (see figure 13). The resulting structures strongly depend on the initial distribution of the holes. A merging of drops for example was simulated on low energy and heterogeneous surfaces [185]. In principle the wavelength of the Rayleigh instabilities determines the distance between neighbouring drops and in principle all drops should have equal size. As observed experimentally smaller and larger drops most probably alternate (see figure 1(d)). This is caused by a periodic local reduction of the width of the liquid cylinder due to the instability and the resulting decrease of the wavelength of the unstable mode.

4.4. Late stages

In the late stages of the dewetting process isolated drops have formed on the surface. Initially, these drops still exhibit a non-equilibrium shape, which is characterized by a non-minimized energy density. As a consequence the three phase contact line deviates from the equilibrium

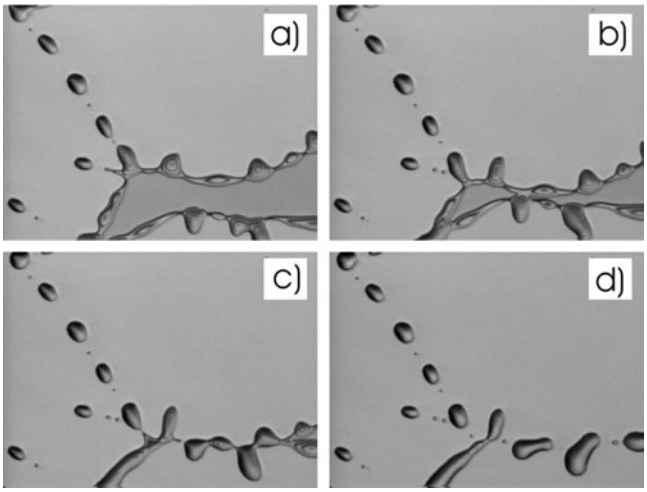

Figure 13. Dewetting of PS from a Si surface as investigated by OM: the time series covers 945 s. The surface covered with a homogeneous PS film appears darker as compared to the bare Si. Due to the height of the drops interference patterns are visible. Reproduced with permission from [116].

condition determined by the contact angle θ. In equilibrium the polymeric drop is given by a full sphere out of which a section is cut by the solid substrate underneath the drop, yielding a spherical cap described by Young's equation $\gamma_{\mathrm{lv}} \cos\theta = \gamma_{\mathrm{sv}} - \gamma_{\mathrm{sl}}$ [186]. The assumption of a cylindrical symmetry of the drop is expressed in the radial dependence of the drop height. Within the assumption of a chemical potential difference between bulk liquid and vapour phase $\Delta\mu \to 0$, the drop profile can be solved for analytically [187]. The local height of the liquid–vapour interface above the solid substrate is given by $h(r) = F(1 - (r/R)^2)$ with the drop height F and the drop radius R fulfilling $F/R = \sqrt{|S|/(2\gamma_{\mathrm{lv}})}$ [29]. In addition, forces which compete with the interfacial tensions have to be taken into account. Gravity, mostly relevant for very large drops, yields a flattening of the central part. For small droplets gravity is negligible but intermolecular forces become dominant. The contact line tension τ, defined by the excess free energy per unit length of the contact line, has to be taken into account. It describes the curvature κ of the three phase contact line and causes a change of the contact angle $\cos\theta_\tau = \cos\theta - \tau\kappa/\gamma_{\mathrm{lv}}$ [188] and basically effects the shape of the drop near the contact line [29].

Figure 14 shows an example of changes in the contact line as detected with SFM. An initially confined homogeneous P(S-*b*-pMS) diblock copolymer film was destabilized by annealing under toluene vapour. After 4 h polymeric islands have formed on the native oxide of the Si, whereas it took considerably longer to round the droplet shape. After 12 h the contact line became more circular but still not all droplets exhibited this shape. In addition the height had increased slightly [197].

Experimentally contact angles have been measured for a large number of systems over decades. Within this review we restrict consideration to some selected values experimentally observed after the dewetting of an initially homogeneous polymer film.

Droplets of PS on Si with 191 nm thermally oxidized Si exhibited a contact angle of 6.9° and central heights of 20–40 nm, whereas on octadecyltrichlorsilane (OTS) covered Si an angle of about 58° and central heights of 200–550 nm were measured [29]. In [30] from dewetting of 5.0 nm of PS on thermally oxidized Si ($h = 191$ nm) a contact angle of 7.5°, on MgF_2

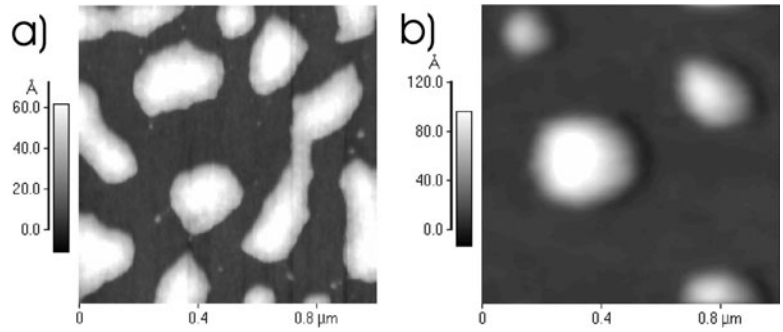

Figure 14. SFM pictures displaying the droplet shape after (a) 4 h and (b) 12 h of annealing under toluene vapour of a confined P(S-*b*-pMS) diblock copolymer film on Si with a native oxide layer. Each SFM picture shows a scan range of $1 \times 1\ \mu m^2$ [189]

($h = 5.4$ nm) a contact angle of 15° and on Au no dewetting at all (meaning $\theta = 0$) were reported. On TiN PS exhibited 11°, PMMA 22° and a symmetric diblock copolymer of both P(S-*b*-MMA) 21° [80]. Contact angles of PS drops on top of PS brushes were reported to differ between 5° and 8° depending on the type of bimodal brush prepared [107].

Drops of the diblock copolymer P(S-*b*-MMA) on native oxide covered Si showed contact angles of 14°, while on a brush layer by itself the value reduced to 1.5° [80]. For statistical random copolymers of diethylene and ethylethylene monomers dewetting from a cross-linked network by itself typical contact angles of 5.5°–6° were measured with SFM and OPIM [190]. PS droplets on P(S-*b*-VP) block copolymer surfaces showed contact angles of 3.4° [58].

During the self-dewetting of perfluoroalkaly-methylacrylate films on glass substrates contact angles of 15°–23° for the growing drops were determined with SFM [72]. Subsequently, layer after layer coagulated and the size of the drops increased by including the material which was contained in the collapsed layer. A complete dewetting of the substrate was not reached, but a thin layer of approximately one and a half bilayer spacings remained, implying that the contact angles were measured against this remaining polymeric layer.

In bilayer films of PS dewetting from PMMA and increase of the contact angle from 92° to 96° were achieved by the addition of fluorocarbon-terminated PS to the top layer [65].

Very large contact angles were reported in the dewetting of polyethylenepropylene (PEP) from PS and PMMA substrates when immersed in aliphatic alcohols [191]. Irrespective of the type of alcohol on PMMA contact angles of 180° were detected, whereas on PS the contact angle varied between 75° and 180°.

Only in the case of homopolymer drops is the contact angle sufficient information. For more complex polymers such as diblock copolymers as well as for polymer blends which created drops or droplets, the internal arrangement of the molecules inside the drop is important structural information. From the comparison of the topographical information as yielded from SFM with scattering data, structures resulting from phase separation and microphase separation were detected [26, 82, 89, 90, 192]. In the blend of PS and PpMS after annealing, a fried egg-like arrangement of the polymers inside the droplets resulted, in which the polymer with the lower surface tension (PpMS) surrounded the one with the higher surface tension (PS) [89]. In contrast, annealing under toluene vapour atmosphere caused a non-periodic random phase separation structure inside the droplets [90] and an increased monodispersity of the droplet shape. Chemically connecting the polymers PS and PpMS resulted in a diblock copolymer which exhibited a microphase separation structure. The periodic structure was identified as a stretched, perpendicular lamella [82].

In addition to the shape of a single drop and its internal structure the arrangement of all single drops is of interest. For the dewetting of PS from Si with a native oxide layer usually the distribution of the drops forms a pattern of polygons (see figure 1(d)). Thus the parameters required for a description of these patterns are in addition to the diameter of the drops, the number of drops per reference area and the diameter of the polygons [27]. Typically, power law dependences were observed with corresponding exponents, which however differ as a function of the wettability of the substrate surface [27, 28]. As discussed by Stange *et al* [31] the polygon pattern exhibits remarkable similarities with computer-generated Voronoi tessellations [193]. One way of generating a Voronoi tessellation starts with Poisson points randomly distributed on a surface. The points simultaneously expand in circular discs at the same rate and no disc is allowed to impinge on the area of another and so must deform upon further expansion. Hence, the discs evolve into polygons, each edge of which is equidistant from two Poisson points and each vertex equidistant from three Poisson points. As a consequence, important criteria are an average number of edges of the polygon of six and an average angle between edges of 120° [194]. Both criteria were met in the case of ultrathin [31] and thin [27] PS films on Si with a native oxide layer. The Voronoi type of construction means that rupture starts from nucleation points almost simultaneously. The Poisson type of distribution of the points fits to the Minkowski measures based type of analysis of Jacobs *et al* [152] and is a typical sign of a nucleated instead of a spinodal dewetting process. Thus within this type of analysis the presence of a polygon pattern of drops can be understood as a strong hint of the absence of a spinodal process. Anyway, it should be clear that the final arrangement of drops can never replace kinetic analysis, which is the only sure proof of any of the destabilizing mechanisms.

The arrangement of drops into a polygon pattern is not restricted to homopolymers. It was observed in the case of liquid crystalline [76] and diblock copolymer films [77] as well. In both cases heterogeneous nucleation was assigned as a corresponding destabilization process. For the model system of a dewetting silicon oil film from nanoheterogeneous surfaces Haidara *et al* [39] pictured different types of drop arrangement including the polygon pattern. As a function of the surface type different assemblies of the drops were found. As shown in [93] even the system PS on native oxide covered Si allowed patterns deviating from the polygon type one in the case where the solvent toluene is replaced by tetrahydrofuran (THF). A pattern comparable to the so-called wetting–dewetting case was observed.

As regards the dynamics, from x-ray scattering evidence for capillary waves on dewetted polymer film surfaces was reported [133]. On top of PEP islands surface waves were detected. The propagation of the waves is suppressed by the background van der Waals potential and superimposed over the island structure.

5. Pattern formation

In the case of homopolymer films dewetting is basically the only self-organizing process yielding pattern formation. On the basis of mass conservation and following the simple scaling arguments of the destabilization routes it was successfully applied in the preparation of nanostructured polymeric surfaces [24, 26]. Both major dewetting processes—spinodal decomposition and nucleation–growth—give rise to an increase of the most prominent in-plane length scale with increasing thickness of the initial film. In a dewetting scenario the most prominent in-plane length is given by the distance between isolated drops. In addition the drop diameter and the drop distance are correlated. With decreasing drop distance the drop diameter decreases as well and frequently the description ‘drop’ is replaced by ‘droplet’. To enter the regime of nanostructures the initial films used have to have extremely small thicknesses. Due to the film thickness being small compared to the radius of gyration R_g of the

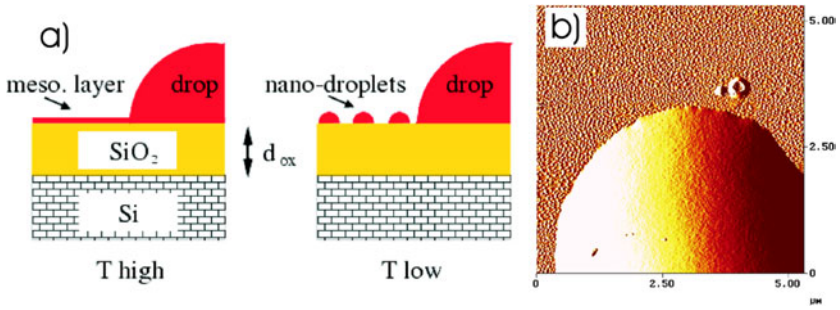

Figure 15. (a) A schematic drawing of a PS film on top of a Si substrate covered with an oxide layer of thickness d_{ox}. At high temperatures macroscopic drops sit on top of a mesoscopic film. At low temperatures this mesoscopic film becomes unstable and ruptures into nanodroplets. Reproduced from [15]. (b) An SFM error signal showing the coexistence of large drops and nanodroplets, from [24].

unperturbed molecule, the films are confined as regards the spatial dimension perpendicular to the substrate surface.

As shown by Zhao *et al* [134], from the dewetting of confined PEP ($M_w = 290$k, $h = 7.3$–18.3 nm) films droplets with diameters of the order of 1 μm result. Due to the different sizes of the droplet height as compared to the much larger droplet diameter the resulting shape was called pancake type. For the system PS ($M_w = 157$k) on native oxide covered Si the droplet distance scales as a function of film thickness following $\Lambda \sim h^2$ over a film thickness regime covering $R_g/5$ up to R_g [90]. In the case of confined PS/PpMS blend films the same scaling behaviour was detected [86]. In [195] the film thickness range was extended into the non-confined regime exhibiting deviations from this power law. It has to be noted that the spinodal model scaling strictly does not describe the actual film break-up; it is only valid for the early stages. Accordingly, $1/q_m \sim h^2$ does not represent a periodic distance between holes [28]. Nevertheless, the average distance between holes and in the case of confined thin film the droplet distance should remain proportional to h^2. While dewetting morphologies as described above basically cover assemblies of holes or drops and droplets, from the interplay between phase separation and dewetting an increase in richness of morphological features results [26, 89, 109, 195]. Alternatively, the interplay between microphase separation and dewetting in the case of confined diblock copolymer films pursues this idea [81, 82, 136]. For the reverse process, surface patterning by alternative techniques and its application in dewetting we refer the reader to the review by Xia *et al* [196] and references therein.

However, even simple systems such as PS on solid supports enable more complex structures to be produced (see figure 15). In the case of an oxide layer thickness of 2.4 nm a coexistence of large drops and small nanodroplets was observed after dewetting [15, 24, 25, 197]. As calculated via self-consistent field calculations by Müller *et al* [15] the interplay between short and long ranged interactions causes two minima in the effective interface potential. At high temperatures in the melt state the stable minimum gives rise to a mesoscopic homogeneous PS film with large PS drops on top. The presence of this film was proved by x-ray reflectivity [15]. After quenching the sample to low temperatures the second minimum becomes stable and the mesoscopic PS film decays into the observed nanodroplets, while the large drops remain unchanged. For smaller oxide layer thicknesses the mesoscopic layer is no longer stable even at high temperatures and no nanodroplets were observed [24, 27]. As a consequence, the controlled setting of the oxide layer thickness allows the preparation of two coexisting structures with strongly different length scales.

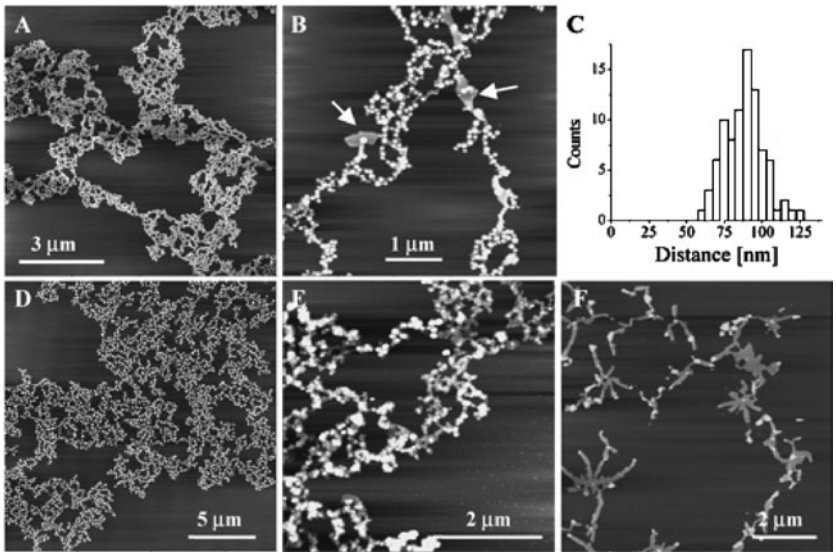

Figure 16. The morphology of PS on mica after exposure of annealed films to an oversaturated water vapour (10 °C, 5 min). Initially the films were prepared from 0.01 mg ml^{-1} PS (molecular weight 10.7k)/toluene solutions: (a), (b) SFM height data, (c) the distribution of distances between neighbouring droplets, (d) with concentration increased by the factor 10, (e), (f) with an increased molecular weight of 500k. Reproduced with permission from [198]. Copyright 2002 American Chemical Society.

A remarkable deviation from the common droplet shape was observed in the water induced dewetting of PS from hydrophilic surfaces [198]. Figure 16 shows examples of aggregate structures formed out of PS on mica after exposure of an initially homogeneous film to oversaturated water. Instead of the common droplet shape the structure appeared to be fractal with a large contact line. From a variation of the PS concentration used during the preparation of the PS films or of the molecular weight, modifications of the structures resulted. The suggested model starts with the nucleation of water at randomly distributed nucleation sites. Next, the water droplets increase in size, displacing the PS film due to the hydrophilic character of the substrate, in a non-uniform process. This causes a thickening of the remaining polymer until it becomes so immobile that the displacement process stops. In contrast to mica on thermally oxidized Si less irregular structures were probed [198].

In addition to surface patterns resulting from a destabilization of an initially homogeneous polymer film, directly after spin coating inhomogeneous films can result. As usual in spin coating, these films exhibit non-equilibrium surface patterns, which of course does not imply that the structures are not reproducible, but annealing will give rise to a kinetic change of the pattern. As regards the convenience of preparation routes the skipping of the subsequent destabilization step however becomes interesting for applications. It is again dewetting which yields the surface pattern, but in contrast to the examples discussed up to now, a highly swollen polymer/solvent film dewets in a radial force field imposed by the spin coating. To pick up the previous example of PS on mica, directly after spin coating droplets were observed which turned into a continuous film after annealing [198]. On top of this film again PS droplets were present.

The absence of a homogeneous film in the case of spin coating highly diluted solutions was reported by Stange *et al* [31]. Different structures starting from molecular and monomolecular

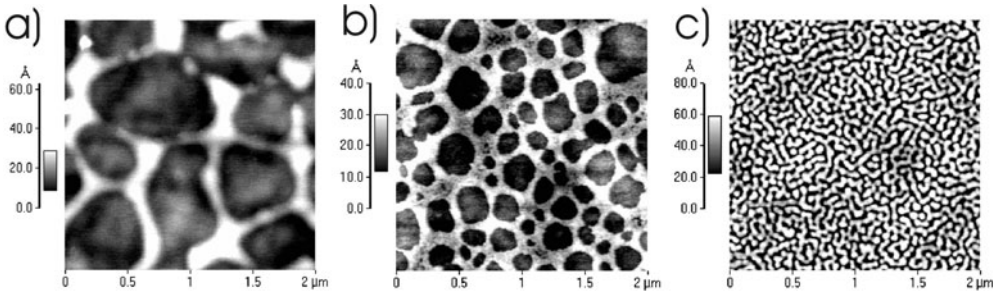

Figure 17. SFM images of PS ($M_w = 207$k) surface patterns resulting directly after spin coating of highly diluted PS/toluene solutions on native oxide covered Si. Each SFM picture shows a scan range of $2 \times 2\ \mu m^2$. From the left to the right the PS concentration increases [199].

particles, via droplets, cellular pattern and small holes were observed with SFM and STM with increasing polymer concentration for PS on Si with a native oxide layer. Comparably, figure 17 shows an example of a surface pattern as measured with SFM directly after spin coating highly diluted PS/toluene solutions [199]. Three different types of structure can be distinguished: PS accumulated in a polygon pattern (figure 17(a)), holes of different diameter causing a highly ruptured film (figure 17(b)) and a bicontinuous surface pattern which exhibited a strong peak in the Fourier space (figure 17(c)). In particular, the irregularly shaped holes resemble structures which were attributed to the water induced dewetting as discussed above. In contrast the bicontinuous structure would be compatible with a spinodal dewetting and the polygon pattern might originate from nucleation.

For other polymers such as the diblock copolymer poly(styrene-block-isoprene) P(S-*b*-I) after spin coating on top of native oxide covered Si, droplet structures with circular bases result. With increasing polymer concentration the droplet diameter increases. At extremely low concentrations again polygon patterns were observed, whereas no preferred arrangement of the droplets was detected with increasing concentration (see figure 4(a)) [200]. In addition to the topological features as probed with SFM, after spin coating an internal substructure was already detected with scattering techniques; see figure 4(b). It resulted from a microphase separation process and exhibited a stretching of the periodicity as compared to bulk equilibrium structures.

Dewetting can be understood as one possible route for the preparation of well controlled surface patterns. In addition to film instabilities driven by van der Waals forces, instabilities due to electrostatic forces [201–203], elastic forces [204], acoustic instabilities [205], density fluctuations [206, 207] and temperature gradients [208] were reported. In contrast to that for heterogeneous nucleation the signature of the instability is the existence of one dominant wavelength, which yields the film rupture. The force balance between the destabilizing force and the surface tension that tends to minimize the surface area determines this wavelength. As a consequence a controlled instability deviating from the thermal instability enables different surface patterns to arise and the creation of novel structures.

Schäffer *et al* [202] presented a set-up with a polymer film and an air gap in a capacitor device. The polymer is annealed above its glass transition temperature and is thus liquid. The dielectric media experienced a force in an electric field gradient that overcame the surface tension. Inducing an instability based on an electrostatic pressure p_{el} the wavelength of the fastest growing mode is $\lambda_{el} = 2\pi\sqrt{2\gamma/(\partial p_{el}/\partial h)}$. Thus from a variation of the electric field the wavelength in a PS ($M_w = 108$k, $h = 93$, 120 nm), PMMA ($M_w = 98.5$k, $h = 100$ nm) and PBrS ($M_w = 127$k, $h = 125$ nm) film was tuned [203]. In addition the structuring of the top

electrode used yielded a replication of the topographical structure of the electrode enabling the preparation of a pattern decoupled from the surface tension [202]. Lin *et al* [209] extended this dewetting in electrostatic fields to polymeric bilayers. Using a bilayer formed by two different polymers such as PS and PMMA, electrohydrodynamic instabilities at both polymer surfaces produced a hierarchical lateral structure that exhibits two characteristic dimensions [210].

Retaining the set-up of a polymer film with an air gap in between two plates but replacing the electrostatic field by a temperature gradient yielded a second type of instability. Schäffer *et al* [208] applied a laterally homogeneous temperature gradient perpendicular to the polymer–air double layer (PS $M_w = 108$k, $h \cong 100$ nm) of typical values $\Delta T \cong 10$–$55\,^{\circ}$C. The interfacial radiation pressure arising from the heat flow in terms of diffusion of heat through the bilayer destabilizes the film. Columnar and striped patterns were observed, often on the same sample, during annealing. Within the model developed, low frequency waves propagating acoustically are nearly perfectly reflected off the polymer–air interface and cause a destabilizing radiation pressure but conduct only little heat. High frequency modes propagate diffusively, with only little interfacial resistance and essentially establish the steady state heat flux across the bilayer [208]. Experimentally, the characteristic wavelength of the pattern produced varied with the inverse of the initial heat flux J_q through the bilayer $\lambda_{th} \sim 1/J_q$ [211]. The extension towards a lithographical technique again pursued the decoupling from surface tension and temperature gradient driven instabilities were used in pattern replication as well [212].

Placing a elastomer film between two solid walls with a finite air gap towards one wall is a third version of the capacitor set-up, but again without an electric field. Approaching the upper substrate towards the rubber film surface yielded an elastic instability and resulted in the creation of a characteristic pattern [204]. The rubber film thickness and the material parameters such as the Young's modulus determined the evolving typical wavelengths.

Recently, Schäffer and Steiner [205] discussed theoretically the influence of acoustic instabilities in thin polymer films. The acoustic analogue to the Casimir pressure was described as a new destabilizing mechanism. The resulting instability is yet another variation of spinodal dewetting with driving forces comparable to dispersive interactions. For the system of PS on oxidized Si the additional consideration of acoustic forces resulted in a decreased wavelength of the instability. Moreover, for large film thicknesses the crossover behaviour from non-retarded to retarded van der Waals interaction is suppressed. In the case of the extensively investigated system of PS on top of Si with a finite oxide layer thickness a decrease of the wavelength and an extension of the instability region towards slightly larger PS film thicknesses (roughly a factor of $4/3$) was calculated. In addition, a re-entrant instability should occur at thickness larger than 100 nm, which might be anyway difficult to detect due to nucleation effects [205].

In addition the influence of density fluctuations inducing dewetting was calculated [207]. Fluctuations with a sufficiently large amplitude can give rise to a gradient in the disjoining pressure and destabilize the free surface. The example of a binary A–B mixture quenched in a glassy state after deposition by spin coating from a solution is discussed. If both components are miscible, the film formed by spin coating was assumed to have a uniform composition, since the solvent evaporation is too fast to allow for any restructuring. In the case where one component of the mixture has a more favourable interaction with the substrate as compared to the other component, annealing of the sample will cause some diffusion inside the film. This diffusion creates a gradient of concentration across the film, with one component enriched at the substrate. In the case diffusion cannot take place in precisely the same way over the whole film; creation of fluctuations in the mixture composition along the surface might result and yield destabilization [207]. The dewetting of binary mixtures can give rise to more complex pattern as shown by Yarushalmi-Rozen *et al* [92]. Phase separation is followed by a dewetting process proceeding from the sample edges inwards.

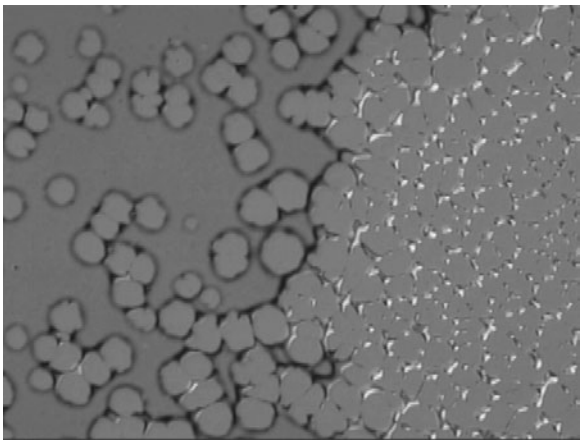

Figure 18. An optical micrograph of the surface of a PS film on top of Si exposed to a temperature gradient. From the left to the right the temperature increases giving rise to a library of different dewetting stages after a fixed time of annealing.

Topographical fluctuations introduced by the mechanical rubbing of the film surface with a rayon cloth were shown to influence the resulting dewetting pattern. Du *et al* [20] chose the model system PS ($M_w = 13.7$k, $h = 6.8$–29.5 nm) on Si with a 106 nm thick thermally oxidized layer and observed an alignment of the drops due to rubbing. The estimated height variation caused by the rubbing was below 10%. Nevertheless, the rubbing produced prominent grooves oriented parallel to the rubbing direction, which pre-aligned the dewetting pattern.

6. Gradient samples

The previous examples were all based on uniform samples; gradient samples provide new opportunities. The idea of using a uniform sample is to have the control parameter such as the film thickness constant over the whole surface of the substrate. During annealing at a fixed temperature the changes in the morphology are measured. As a consequence a large number of individual samples have to be prepared to obtain all transition stages in *ex situ* experiments. In an *in situ* experiment the changes are monitored continuously. Determining the influence of the control parameter requires a repetition of these experiments for a large number of different film thicknesses.

In a gradient sample the film thickness, as a typical control parameter, is no longer constant but changes continuously as a function of the position on the solid support. Thus the gradient sample can be understood as a large number of samples with different film thicknesses, all prepared on top of one surface. Between adjacent samples the control parameter changes only slightly. Based on the idea of a combinatorial characterization, which is successfully applied in many research areas such as pharmaceutical investigations or organic material synthesis, a rapid and systematic generation of experimental data is possible. For a fixed annealing time a library of all dewetting stages results.

Alternatively, in a sample with homogeneous polymer film thickness a gradient can be introduced by applying a temperature gradient during annealing. Figure 18 shows the example of a thin PS ($M_w = 28$k) film which was annealed in a linear temperature gradient. After a fixed annealing time at low temperatures (left part) only the first holes were visible whereas at high temperatures (right part) the final dewetting stages were reached already. Again a library of all dewetting stages and the transition stages resulted [213].

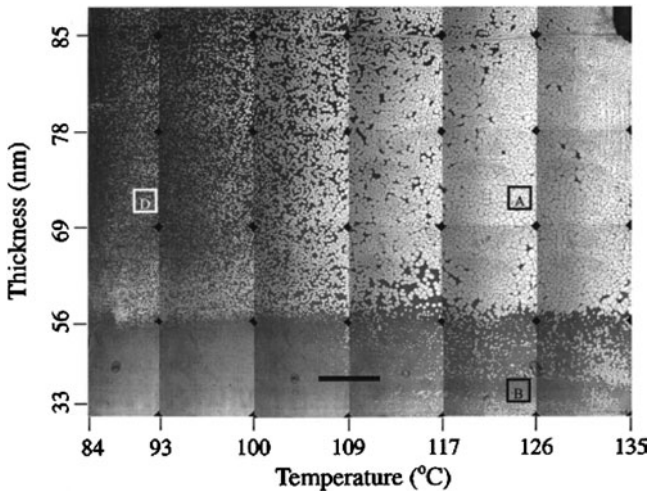

Figure 19. A composite of optical images displaying the dewetting of PS on top of Si in an orthogonal gradient of film thickness and annealing temperature. The overall wetted and dewetted pattern features are in fact visible as dark and bright regions, respectively, to the unaided eye. The scale bar denotes 2.0 ± 0.1 mm. Reproduced with permission from [154]. Copyright 2000 American Chemical Society.

Creating two orthogonal gradients follows the pathway of combinatorial research and creates so-called two dimensional libraries. As regards dewetting the most natural orthogonal gradients are the film thickness and the annealing temperature. As demonstrated by Karim and co-workers [154] for the example of PS ($M_w = 1.9$k) on Si the common dewetting patterns observed in non-combinatorial studies were reproduced. Figure 19 shows a resulting composite of optical images. The thickness range covered was 33–85 nm and temperature was varied between 84 and 135 °C. Due to the relatively weak gradients chosen, no appreciable flow of polymer film over the experimental timescale was induced. For significantly steeper gradients flow will be no longer negligible.

For a detailed analysis SFM was applied. High throughput screening was only performed with OM. However, this screening enabled the detection of positions which were identified as being interesting as regards the dewetting [154]. For future work other gradients such as surface chemistry and molecular weight changes will be interesting for investigations concerning dewetting. One example is illustrated by the preparation of a contact angle variation along a gradient superimposed on an orthogonal film thickness gradient [214].

7. Conclusions

To summarize, with the large body of experimental work on the dewetting of thin polymer films a significantly deeper understanding of film destabilization was achieved. In addition, dewetting turned out to be a powerful technique for the preparation of patterned substrates covering the regime of nanostructured surfaces as well. However, despite all the progress open questions still remain and new questions arise (see the forthcoming work [215]).

Acknowledgments

This work has benefited strongly from fruitful and enjoyable collaborations with K Binder, J S Gutmann, M Müller, W Petry, M Stamm and O Wunnicke. The cooperation of E Bauer,

A Götzendorfer, N Hermsdorf, V Lauter, S Loi, C Lorenz-Haas, E Maurer, P Panagiotou, T Titz, P Volodin and M Wolkenhauer in many experiments and stimulating discussions with R Blossey, H J Butt, M D Foster, K Graf, S Herminghaus, K Jacobs, A Karim, G Krausch, G Reiter and T Thurn-Albrecht is gratefully acknowledged. Support at HASYLAB was provided by S Cunis, M Dommach, W Fenzl, S S Funari, R Gehrke, G von Krosigk and A Meyer, at ILL by R Cubitt and at ESRF by M Burghammer, C Riekel, S Roth and D Smilgies. The silicon substrates used were kindly made available by Wacker Siltronic, Burghausen (Germany). Financial support was provided by the DFG in the framework of the priority programme 'wetting and structure formation at interfaces' (Sta324/8).

References

[1] Dietrich S 1988 *Phase Transitions and Critical Phenomena* vol 12 (New York: Academic)
[2] Israelachvili J N 1991 *Intermolecular and Surface Forces* 2nd edn (London: Academic)
[3] Müller M, Binder K and Albano E V 2001 *Int. J. Mod. Phys.* B **15** 1867
[4] Binder K, Landa D and Müller M 2003 *J. Stat. Phys.* **110** 1411
[5] Lawrence C J 1988 *Phys. Fluids* **31** 2786
[6] Schubert D W 1997 *Polym. Bull.* **38** 177
[7] Vrij A and Overbeek J T G 1968 *J. Am. Chem. Soc.* **90** 3074
[8] Thile U, Velarde M G and Neuffer K 2001 *Phys. Rev. Lett.* **87** 016104
[9] Thile U, Neuffer K, Pomeau Y and Velarde M G 2002 *Colloids Surf.* A **206** 135
[10] Cazabat A M 1990 *Liquids at Interfaces* (*Les Houches Session Series*) ed J Charvolin, J F Joanny and J Zinn-Justin (Amsterdam: Elsevier)
[11] Findenegg G H and Herminghaus S 1997 *Curr. Opin. Colloid Interface Sci.* **2** 301
[12] Müller-Buschbaum P, Casagrande M, Gutmann J, Kuhlmann T, Stamm M, Cunis S, von Krosigk G, Lode U and Gehrke R 1998 *Europhys. Lett.* **42** 517
[13] Müller M and MacDowell L G 2003 *J. Phys.: Condens. Matter* **15** R609
[14] Geoghegan M and Krausch G 2003 *Prog. Polym. Sci.* **28** 261
[15] Müller M, MacDowell L G, Müller-Buschbaum P, Wunnicke O and Stamm M 2001 *J. Chem. Phys.* **115** 9960
[16] Seemann R, Herminghaus S and Jacobs K 2001 *Phys. Rev. Lett.* **86** 5534
[17] Bischof J, Scherer D, Herminghaus S and Leiderer P 1996 *Phys. Rev. Lett.* **77** 1536
[18] Han G C, Wu Y H, Luo P, Qiu J J and Chong T C 2003 *Solid State Commun.* **126** 479
[19] Feng Y, Karim A, Weiss R A, Douglas J F and Han C C 1998 *Macromolecules* **31** 484
[20] Du B, Xie F, Wang Y, Yang Z and Tsui O K C 2002 *Langmuir* **18** 8510
[21] Henn G, Bucknall D G, Stamm M, Vanhoorne P and Jerome R 1996 *Macromolecules* **29** 4305
[22] Karapanagiotis I, Evans D F and Gerberich W W 2002 *Colloids Surf.* A **207** 59
[23] Lorenz-Haas C, Müller-Buschbaum P, Kraus J, Bucknall D G and Stamm M 2002 *Appl. Phys.* A **74** S383
[24] Müller-Buschbaum P, Vanhoorne P, Scheumann V and Stamm M 1997 *Europhys. Lett.* **40** 655
[25] Müller-Buschbaum P and Stamm M 1998 *Physica* B **248** 229
[26] Müller-Buschbaum P, Gutmann J S and Stamm M 1999 *Phys. Chem. Chem. Phys.* **1** 3857
[27] Reiter G 1992 *Phys. Rev. Lett.* **68** 75
[28] Reiter G 1993 *Langmuir* **9** 1344
[29] Seemann R, Jacobs K and Blossey R 2001 *J. Phys.: Condens. Matter* **13** 4915
[30] Seemann R, Herminghaus S and Jacobs K 2001 *J. Phys.: Condens. Matter* **13** 4925
[31] Stange T G, Mathew R, Evans D F and Hendrickson W A 1992 *Langmuir* **8** 920
[32] Xie R, Karim A, Douglas J F, Han C C and Weiss R A 1998 *Phys. Rev. Lett.* **81** 1251
[33] Yarushalmi-Rozen R, Klein J and Fetters L J 1994 *Science* **263** 793
[34] Yarushalmi-Rozen R and Klein J 1995 *Langmuir* **11** 2806
[35] Jacobs K, Herminghaus S and Mecke K R 1998 *Langmuir* **14** 965
[36] Jacobs K, Seemann R, Schatz G and Herminghaus S 1998 *Langmuir* **14** 4961
[37] Renger C, Müller-Buschbaum P, Stamm M and Hinrichsen G 2000 *Macromolecules* **33** 8388
[38] Sferrazza M, Heppenstall-Butler M, Cubitt R, Bucknall D, Webster J and Jones R A L 1998 *Phys. Rev. Lett.* **81** 5173
[39] Haidara H, Mougin K and Schultz J 2000 *Langmuir* **16** 7773
[40] Herminghaus S, Fery A, Schlagowski S, Jacobs K, Seemann R, Gau H, Mönch W and Pompe T 2000 *J. Phys.: Condens. Matter* **12** A57

[41] Kargupta K, Konnur R and Sharma A 2001 *Langmuir* **17** 1294
[42] Kargupta K and Sharma A 2001 *J. Colloid Interface Sci.* **245** 99
[43] Lenz P, Bechinger C, Schäfle C, Leiderer P and Lipowsky R 2001 *Langmuir* **17** 7814
[44] Mougin K and Haidara H 2003 *Europhys. Lett.* **61** 660
[45] Rehse N, Wang C, Hund M, Geoghegan M, Magerle R and Krausch G 2001 *Eur. Phys. J.* E **4** 69
[46] Rockford L, Liu Y, Mansky P, Russell T P, Yoon M and Mochrie S G J 1999 *Phys. Rev. Lett.* **82** 2602
[47] Gay C 1997 *Macromolecules* **30** 5939
[48] Krausch G 1997 *J. Phys.: Condens. Matter* **9** 7741
[49] Reiter G, Sharma A, Casoli A, David M-O, Khanna R and Auroy P 1999 *Europhys. Lett.* **46** 512
[50] Reiter G, Sharma A, Casoli A, David M-O, Khanna R and Auroy P 1999 *Langmuir* **15** 2551
[51] Ade H, Winesett D A, Smith A P, Andres S, Stammler T, Heske C, Slep D, Rafailovich M H, Sokolov J and Stöhr J 1998 *Appl. Phys. Lett.* **73** 3775
[52] David M O, Reiter G, Sitthai T and Schultz J 1998 *Langmuir* **14** 5667
[53] Faldi A, Composto R J and Winey K I 1995 *Langmuir* **11** 4855
[54] Higgins A M and Jones R A L 2000 *Nature* **404** 476
[55] Higgins A M, Sferrazza M, Jones R A L, Jukes P C, Sharp J S, Dryden L E and Webster J 2002 *Eur. Phys. J.* E **8** 137
[56] Krausch G 1996 *Ber. Bunsenges. Phys. Chem.* **98** 446
[57] Lambooy P, Phelan K C, Haugg O and Krausch G 1996 *Phys. Rev. Lett.* **76** 1110
[58] Liu Y, Rafailovich M H, Sokolov J, Schwarz S A, Zhong X, Eisenberg A, Kramer E J, Sauer B B and Satija S 1994 *Phys. Rev. Lett.* **73** 440
[59] Pan Q, Winey K I, Hu H H and Composto R J 1997 *Langmuir* **13** 1758
[60] Pompe T, Fery A and Herminghaus S 1998 *Langmuir* **14** 2585
[61] Qu S, Clarke C J, Liu Y, Rafailovich M H, Sokolov J, Phelan K C and Krausch G 1997 *Macromolecules* **30** 3640
[62] Segalman R A and Grenn P F 1999 *Macromolecules* **32** 801
[63] Wang C, Krausch G and Geoghegan M 2001 *Langmuir* **17** 6269
[64] Wunnicke O, Lorenz-Haas C, Müller-Buschbaum P, Leiner V and Stamm M 2002 *Appl. Phys.* A **74** S445
[65] Yuan C, Ouyang M and Koberstein J T 1999 *Macromolecules* **32** 2329
[66] Martin A, Buguin A and Brochard-Wyart F 2001 *Langmuir* **17** 6553
[67] Martin A, Buguin A and Brochard-Wyart F 2002 *Europhys. Lett.* **57** 604
[68] Bardon S, Valignat M P, Cazabat A M, Stocker W and Rabe J P 1998 *Langmuir* **14** 2916
[69] Demirel A L and Jerome B 1999 *Europhys. Lett.* **45** 58
[70] Herminghaus S, Jacobs K, Mecke K, Bischof J, Fery A, Ibn-Elhaj M and Schlagowski S 1998 *Science* **282** 916
[71] Schlagowski S, Jacobs K and Herminghaus S 2002 *Europhys. Lett.* **57** 519
[72] Sheiko S, Lermann E and Möller M 1996 *Langmuir* **12** 4015
[73] Valignat M P, Villette S, Li J, Barberi R, Bartolino R, Dubois-Violette E and Cazabat A M 1992 *Phys. Rev. Lett.* **77** 1994
[74] Vandenbrouck F, Valignat M P and Cazabat A M 1999 *Phys. Rev. Lett.* **82** 2693
[75] Vix A, Müller-Buschbaum P, Stocker W, Stamm M and Rabe J P 2000 *Langmuir* **16** 10456
[76] van der Wielen M W J, Stuart Cohen M A and Fleer G J 1998 *Langmuir* **14** 7065
[77] Hamley I W, Hiscutt E L, Yang Y-W and Booth C 1999 *J. Colloid Interface Sci.* **209** 255
[78] Limary R and Green P F 1999 *Macromolecules* **32** 8167
[79] Limary R and Green P F 1999 *Langmuir* **15** 5617
[80] Limary R, Green P F and Shull K R 2002 *Eur. Phys. J.* E **8** 103
[81] Müller-Buschbaum P, Gutmann J S, Lorenz-Haas C, Mahltig B, Stamm M and Petry W 2001 *Macromolecules* **34** 7463
[82] Müller-Buschbaum P, Gutmann J S, Lorenz-Haas C, Wunnicke O, Stamm M and Petry W 2002 *Macromolecules* **35** 2017
[83] Peters R D, Yang X M, Kim T K, Sohn B H and Nealey P F 2000 *Langmuir* **16** 4625
[84] Carre A and Shanahan M E R 1997 *J. Colloid Interface Sci.* **191** 141
[85] Cho K, Seo K H, Ahn T O, Kim J and Kim K U 1997 *Polymer* **38** 4825
[86] Gutmann J S, Müller-Buschbaum P, Wunnicke O and Stamm M 1997 *Mater. Res. Soc. Symp. Proc.* **629** 6.1
[87] Geoghegan M, Ermer H, Jüngst G, Krausch G and Brenn R 2000 *Phys. Rev.* E **62** 940
[88] Müller-Buschbaum P, Gutmann J S and Stamm M 1999 *J. Macromol. Sci.* B **38** 577
[89] Müller-Buschbaum P, Gutmann J S, Cubitt R and Stamm M 1999 *Colloid Polym. Sci.* **277** 1193

[90] Müller-Buschbaum P, Gutmann J S, Stamm M, Cubitt R, Cunis S, von Krosigk G, Gehrke R and Petry W 2000 *Physica* B **283** 53
[91] Müller-Buschbaum P, Gutmann J S and Stamm M 2000 *Macromolecules* **33** 4886
[92] Yarushalmi-Rozen R, Kerle T and Klein J 1999 *Science* **285** 1254
[93] Müller-Buschbaum P and Stamm M 1998 *Macromolecules* **31** 3686
[94] Bornside D E, Macosko C W and Scriven L E 1987 *J. Imaging Technol.* **13** 122
[95] Oron A, Davis S H and Bankoff S G 1997 *Rev. Mod. Phys.* **69** 931
[96] Meyerhofer D 1978 *J. Appl. Phys.* **49** 3993
[97] Spangler L L, Torkelson J M and Poyal J S 1990 *Polym. Eng. Sci.* **30** 644
[98] Müller-Buschbaum P, Gutmann J S, Kraus J, Walter H and Stamm M 2000 *Macromolecules* **33** 569
[99] Müller-Buschbaum P, Gutmann J S, Wolkenhauer M, Kraus J, Stamm M, Smilgies D and Petry W 2001 *Macromolecules* **34** 1396
[100] Strawhecker K E, Kumar S K, Douglas J F and Karim A 2001 *Macromolecules* **34** 4669
[101] Müller-Buschbaum P, Gutmann J S, Lorenz C, Schmitt T and Stamm M 1998 *Macromolecules* **31** 9265
[102] Kraus J, Müller-Buschbaum P, Bucknall D G and Stamm M 1999 *J. Polym. Sci. Phys.* **37** 2862
[103] Gutmann J S, Müller-Buschbaum P, Schubert D W, Stribeck N, Smilgies D and Stamm M 2000 *Physica* B **283** 40
[104] Vix A, Müller-Buschbaum P and Stamm M 2003 at press
[105] Foster M D, van Krosigk G, Ponomarenko K, Ruehe J and Müller-Buschbaum P 2003 at press
[106] Fondecave R and Brochard-Wyart F 1998 *Macromolecules* **31** 9305
[107] Reiter G, Auroy P and Auvray L 1996 *Macromolecules* **29** 2150
[108] Kerle T, Yarushalmi-Rozen R, Klein J and Fetters L J 1998 *Europhys. Lett.* **44** 484
[109] Müller-Buschbaum P, O'Neil S A, Affrossman S and Stamm M 1998 *Macromolecules* **31** 5003
[110] Reiter G 1994 *Macromolecules* **27** 3046
[111] Müller-Buschbaum P, Gutmann J S, Stamm M and Cubitt R 2000 *Macromol. Symp.* **149** 283
[112] Magonov S N and Whangbo M H 1996 *Surface Analysis with the STM and AFM* (Weinheim: VCH)
[113] Cappella B and Dietler G 1999 *Surf. Sci. Rep.* **34** 1
[114] Sheiko S S 2000 *Adv. Polym. Sci.* **151** 61
[115] Knoll A, Magerle R and Krausch G 2001 *Macromolecules* **34** 4159
[116] Lorenz C 1997 *Thesis* University of Mainz
[117] Magerle R 2000 *Phys. Rev. Lett.* **85** 2749
[118] Parrat L G 1954 *Phys. Rev.* **55** 359
[119] Born M and Wolf E 1964 *Principles of Optics* (Oxford: Pergamon)
[120] James R W 1962 *The Optical Principles of the Diffraction of X-Rays* (Woodbridge, CN: OxBow)
[121] Lekner J 1987 *Theory of Reflection* (Dordrecht: Martinus Nijhoff)
[122] Kunz K, Reiter J, Götzelmann A and Stamm M 1993 *Macromolecules* **26** 4316
[123] Stamm M and Schubert D W 1995 *Annu. Rev. Mater. Sci.* **25** 325
[124] Stamm M 2000 *Scattering in Polymeric and Colloidal Systems* ed W Brown and K Mortensen (Amsterdam: Gordon and Breach)
[125] Reiter G 1993 *Europhys. Lett.* **23** 579
[126] Daillant J and Bélorgey O 1992 *J. Chem. Phys.* **97** 5824
[127] Holý V and Baumbach T 1994 *Phys. Rev.* B **49** 10668
[128] Sinha S K, Sirota E B, Garoff S and Stanley H B 1988 *Phys. Rev.* B **38** 2297
[129] Pynn R 1992 *Phys. Rev.* B **45** 602
[130] Salditt T, Metzger T H, Peisl J and Goerigk G 1995 *J. Phys. D: Appl. Phys.* **28** A236
[131] Naudon A, Babonneau D, Thiaudiere D and Lequien S 2000 *Physica* B **283** 69
[132] Tolan M 1999 *X-ray Scattering from Soft-Matter Thin Films* (*Springer Tracts in Modern Physics* vol 148) (Berlin: Springer)
[133] Tolan M, Seeck O H, Schlomka J P, Press W, Wang J, Sinha S K, Li Z, Rafailovich M H and Sokolov J 1998 *Phys. Rev. Lett.* **81** 2731
[134] Zhao W, Rafailovich M H, Sokolov J, Fetters L J, Plano R, Sanyal M K and Sinha S K 1993 *Phys. Rev. Lett.* **70** 1453
[135] Müller-Buschbaum P 2003 *Anal. Bioanal. Chem.* **376** 3
[136] Müller-Buschbaum P, Wolkenhauer M, Wunnicke O, Stamm M, Cubitt R and Petry W 2001 *Langmuir* **17** 5567
[137] Kerle T, Lin Z, Kim H-C and Russel T P 2001 *Macromolecules* **34** 3484
[138] Andelmann D, Joanny J F and Robbins M O 1988 *Europhys. Lett.* **7** 731
[139] Brochard F and Daillant J 1990 *Can. J. Phys.* **68** 1084

[140] Brochard-Wyart F, Redon C and Sykes C 1992 *C. R. Acad. Sci., Paris* II **19** 314
[141] Wunnicke O, Müller-Buschbaum P and Stamm M 2003 at press
[142] Yoneda Y 1963 *Phys. Rev.* **131** 2010
[143] Sharma A and Ruckenstein E 1989 *J. Colloid Interface Sci.* **133** 358
[144] Sharma A and Ruckenstein E 1990 *J. Colloid Interface Sci.* **137** 433
[145] Liu H, Bhattacharya A and Chakrabarti A 1998 *J. Chem. Phys.* **109** 8607
[146] Karapanagiotis I, Fennell Evans D and Gerberich W W 2001 *Macromolecules* **34** 3741
[147] Karapanagiotis I, Fennell Evans D and Gerberich W W 2001 *Langmuir* **17** 3266
[148] Jacobs K 1997 *UFO Dissertation* vol 311, Konstanz University
[149] Seemann R 2001 *PhD Thesis* Ulm University
[150] Reiter G and de Gennes P G 2001 *Eur. Phys. J.* E **6** 25
[151] Croll S G 1979 *J. Appl. Polym. Sci.* **23** 848
[152] Jacobs K, Seemann R and Mecke K 2000 *Dynamics of Structure Formation in Thin Liquid Films: a Special Spatial Analysis* ed K Mecke and D Stoyan (Heidelberg: Springer)
[153] Mecke K R 1994 *Integralgeometrie in der Statistischen Physik—Perkolation, Komplexe Flssigkeiten und die Struktur des Universums* (*Reihe Physik* vol 25) (Frankfurt: Harri Deutsch)
[154] Meredith J C, Smith A P, Karim A and Amis E J 2000 *Macromolecules* **33** 9747
[155] Konnur R, Kargupta K and Sharma A 2000 *Phys. Rev. Lett.* **84** 931
[156] Kerle T, Yarushalmi-Rozen R and Klein J 1997 *Europhys. Lett.* **38** 207
[157] Kerle T, Yarushalmi-Rozen R and Klein J 1998 *Macromolecules* **31** 422
[158] Reiter G, Schultz J, Auroy P and Auvray L 1996 *Europhys. Lett.* **33** 29
[159] Reiter G, Khanna R and Sharma A 2003 *J. Phys.: Condens. Matter* **15** S331
[160] Sharma A 1993 *Langmuir* **9** 861
[161] Sharma A 1993 *Langmuir* **9** 3580
[162] Seemann R, Herminghaus S and Jacobs K 2001 *Phys. Rev. Lett.* **87** 196101
[163] Reiter G 2001 *Phys. Rev. Lett.* **87** 186101
[164] Brochard-Wyart F, Martin P and Redon C 1993 *Langmuir* **9** 3682
[165] Brochard-Wyart F, de Gennes P G, Hervert H and Redon C 1994 *Langmuir* **10** 1566
[166] Brochard-Wyart F, Gay C and de Gennes P G 1996 *Macromolecules* **29** 377
[167] Brochard-Wyart F, Debregeas G, Fondecave R and Martin P 1997 *Macromolecules* **30** 1211
[168] Choi S H and Zhang Newby B 2003 *Langmuir* **19** 1419
[169] Haidara H, Vonna L and Schultz J 1998 *Langmuir* **14** 3425
[170] Oslanec R, Costa A C and Composto R J 2000 *Macromolecules* **33** 5505
[171] Reiter G 2002 *Eur. Phys. J.* E **8** 251
[172] Redon C, Brzoska J B and Brochard-Wyart F 1994 *Macromolecules* **27** 468
[173] Reiter G and Khanna R 2000 *Langmuir* **16** 6351
[174] Kolmogorov A N 1937 *Izv. Akad. Nauk SSSR Otd. Mat.* **3** 335
[175] Avrami M 1939 *Chem. Phys.* **7** 1103
[176] Herminghaus S 2002 *Phys. Rev. Lett.* **89** 056102
[177] Orts W J, van Zanten J H, Wu W and Satija S K 1993 *Phys. Rev. Lett.* **71** 867
[178] Stange T G, Evans D F and Hendrickson W A 1997 *Langmuir* **13** 4459
[179] Reiter G and Khanna R 2000 *Phys. Rev. Lett.* **85** 2753
[180] Saulnier F, Raphael E and de Gennes P G 2002 *Phys. Rev. Lett.* **88** 196101
[181] Saulnier F, Raphael E and de Gennes P G 2002 *Phys. Rev.* E **66** 061607
[182] Becker J, Grün G, Seemann R, Mantz H, Jacobs K, Mecke K R and Blossey R 2003 *Nature Mater.* **2** 59
[183] Neto C, Jacobs K, Seemann R, Blossey R, Becker J and Grün G 2003 *J. Phys.: Condens. Matter* **15** 421
[184] Gau H, Herminghaus S, Lenz P and Lipowsky R 1999 *Science* **283** 47
[185] Schwartz L W and Eley R R 1998 *J. Colloid Interface Sci.* **202** 173
[186] Young T 1805 *Phil. Trans. R. Soc.* **35** 95
[187] Bausch R and Blossey R 1993 *Phys. Rev.* E **48** 1131
[188] Pompe T and Herminghaus S 2000 *Phys. Rev. Lett.* **85** 1930
[189] Müller-Buschbaum P, Cubitt R and Petry W 2003 *Langmuir* at press
[190] Kerle T, Cohen S R and Klein J 1997 *Langmuir* **13** 6360
[191] Shull K R and Karis T E 1994 *Langmuir* **10** 334
[192] Müller-Buschbaum P, Cubitt R and Petry W 2002 *Appl. Phys.* A **74** S342
[193] Voronoi G J 1908 *Reine Angew. Math.* **134** 198
[194] Weaire D and Rivier N 1984 *Contemp. Phys.* **25** 59
[195] Müller-Buschbaum P and Stamm M 2001 *Colloid Polym. Sci.* **279** 376

[196] Xia Y, Qin D and Yin Y 2001 *Curr. Opin. Colloid Interface Sci.* **6** 54
[197] Müller-Buschbaum P, Roth S V, Burghammer M, Diethert A, Panagiotou P and Riekel C 2003 *Europhys. Lett.* **61** 639
[198] Bonaccurso E, Butt H J, Franz V, Graf K, Kappl M, Loi S, Chemitz S, Böhm M, Petrova B, Jonas U and Spiess H W 2002 *Langmuir* **18** 8056
[199] Götzendorfer A, Müller-Buschbaum P and Petry W 2003 at press
[200] Müller-Buschbaum P, Hermsdorf N, Gutmann J S, Stamm M, Cunis S, Gehrke R and Petry W 2003 at press
[201] Herminghaus S 1999 *Phys. Rev. Lett.* **83** 2359
[202] Schäffer E, Thurn-Albrecht T, Russell T P and Steiner U 2000 *Nature* **403** 874
[203] Schäffer E, Thurn-Albrecht T, Russell T P and Steiner U 2001 *Europhys. Lett.* **53** 518
[204] Mönch W and Herminghaus S 2001 *Europhys. Lett.* **53** 525
[205] Schäffer E and Steiner U 2002 *Eur. Phys. J.* E **8** 347
[206] Sharma A and Mittal J 2002 *Phys. Rev. Lett.* **89** 186101
[207] Wensink K D F and Jerome B 2002 *Langmuir* **18** 413
[208] Schäffer E, Harkema S, Blossey R and Steiner U 2002 *Europhys. Lett.* **60** 255
[209] Lin Z, Kerle T, Russell T P, Schäffer E and Steiner U 2002 *Macromolecules* **35** 6255
[210] Morariu M D, Voicu N E, Schäffer E, Lin Z, Russell T P and Steiner U 2003 *Nature Mater.* **2** 48
[211] Schäffer E, Harkema S, Roerdink M, Blossey R and Steiner U 2003 *Macromolecules* **36** 1645
[212] Schäffer E, Harkema S, Roerdink M, Blossey R and Steiner U 2003 *Adv. Mater.* **16** 514
[213] Titz T and Müller-Buschbaum P 2003 at press
[214] Ashley K M, Meredith J C, Amis E, Raghavan D and Karim A 2003 *Polymer* **44** 769
[215] Reiter G (ed) *Eur. Phys. J.* E (focus point: unstable thin films)